Impact of mineral dust on shortwave and longwave radiation: evaluation of different vertically-resolved parameterizations in 1-D radiative transfer computations

María José Granados-Muñoz[1], Michael Sicard[1,2], Roberto Román[3], Jose Antonio Benavent-Oltra[4,5], Rubén Barragán[1,2], Gerard Brogniez[6], Cyrielle Denjean[7,8], Marc Mallet[7], Paola Formenti[8], Benjamín Torres[6,9] and Lucas Alados-Arboledas[4,5]

[1] Remote Sensing Laboratory / CommSensLab, Universitat Politècnica de Catalunya, Barcelona, 08034, Spain
[2] Ciències i Tecnologies de l'Espai - Centre de Recerca de l'Aeronàutica i de l'Espai / Institut d'Estudis Espacials de Catalunya (CTE-CRAE / IEEC), Universitat Politècnica de Catalunya, Barcelona, 08034, Spain
[3] Grupo de Óptica Atmosférica (GOA), Universidad de Valladolid, Valladolid, Spain.
[4] Department of Applied Physics, University of Granada, 18071 Granada, Spain
[5] Andalusian Institute for Earth System Research (IISTA-CEAMA), University of Granada, Autonomous Government of Andalusia, 18006 Granada, Spain
[6] Laboratoire d'Optique Atmosphérique, University of Lille 1, Villeneuve d'Ascq, France
[7] CNRM, Centre National de la Recherche Météorologique (UMR3589, CNRS, Météo-France), Toulouse, France
[8] LISA, UMR CNRS 7583, Université Paris Est Créteil et Université Paris Diderot, Institut Pierre-Simon Laplace, Créteil, France
[9] GRASP-SAS, Remote sensing developments, LOA/Université Lille-1, Villeneuve d'Ascq, France

Correspondence to: Maria Jose Granados (maria.jose.granados@tsc.upc.edu)

Abstract.

Aerosol radiative properties are investigated in southeastern Spain during a dust event on June 16-17, 2013 in the framework of the ChArMEx/ADRIMED (Chemistry-Aerosol Mediterranean Experiment /Aerosol Direct Radiative Impact on the regional climate in the MEDiterranean region) campaign. Particle optical and microphysical properties from ground-based sun/sky photometer and lidar measurements, as well as in situ measurements onboard the SAFIRE ATR 42 French research aircraft are used to create a set of different levels of input parameterizations, which feed the 1-D radiative transfer model (RTM) GAME (Global Atmospheric ModEl). We consider three datasets: 1) a first parameterization based on the retrievals by an advanced aerosol inversion code (GRASP; Generalized Retrieval of Aerosol and Surface Properties) applied to combined photometer and lidar data; 2) a parameterization based on the photometer columnar optical properties and vertically-resolved lidar retrievals with the two-component

Klett-Fernald algorithm; and 3) a parameterization based on vertically-resolved optical and microphysical aerosol properties measured in situ by the aircraft instrumentation. Once retrieved, the outputs of the RTM in terms of both shortwave and longwave radiative fluxes are ~~contrasted~~ compared against ground ~~-, satellite~~ and in situ airborne measurements. In addition, the outputs of the model in terms of the aerosol direct radiative effect are discussed with respect to the different input parameterizations. Results show that calculated atmospheric radiative fluxes differ no more than 7 % to the measured ones. The three parameterization datasets produce a cooling effect due to mineral dust both at the surface and the top of the atmosphere. ~~a~~Aerosol radiative effects with differences up to 10 $W \cdot m^{-2}$ in the shortwave spectral range (mostly due to differences in the aerosol optical depth), and 2 $W \cdot m^{-2}$ for the longwave~~-~~ (mainly due to differences in the aerosol optical depth but also to the coarse mode radius used to calculate the radiative properties)~~.~~ are obtained when comparing the three parameterizations. The study reveals the complexity of parametrizing 1-D RTMs as sizing and characterising the optical properties of mineral dust is challenging. The use of advanced remote sensing data and processing, in combination with closure studies on the optical/microphysical properties from in situ aircraft measurements when available, is recommended.

1 Introduction

The radiative effect by atmospheric aerosol is estimated to produce a net cooling effect of the Earth's climate. However, an accurate quantification of this cooling is extremely difficult. In fact, the aerosol radiative effect (ARE) is affected by large uncertainties. Due to the direct aerosol-radiation interaction, the ARE is estimated to be $-0.27\ W \cdot m^{-2}$ on average at the global scale, with an uncertainty range of -0.77 to $-0.23\ W \cdot m^{-2}$, whereas the radiative effect related to cloud adjustments due to aerosols is -0.55 $W \cdot m^{-2}$ (-1.33 to $-0.06\ W \cdot m^{-2}$) (Boucher *et al.*, 2013), being the largest unknown in the radiative forcing of the atmosphere. The extent to which the ARE uncertainty range reported is due to physical processes or due to the measurement ~~artefacts~~ uncertainty itself is still hard to quantify.

In previous studies, the aerosol radiative effects in the longwave (LW) were commonly neglected due to the complexity of an accurate quantification of the optical properties in this spectral range (Roger

et al., 2006; Mallet et al., 2008; Sicard et al., 2012). However, the contribution of the LW component to the ARE is non-negligible for large aerosol particles, i.e., marine aerosol or mineral dust (e.g. Markowicz et al., 2003; Vogelmann et al., 2003; Otto et al., 2007; Perrone and Bergamo, 2011; Sicard et al., 2014a,b; Meloni et al., 2018).

The contribution of mineral dust to the ARE in the infrared spectral range is especially relevant because of its large size and abundance (Meloni et al., 2018). Mineral dust is estimated to be the most abundant aerosol type in the atmosphere by mass (e.g., Ginoux et al., 2012; Choobari et al., 2014), with global emission between 1000 and 3000 $Mt \cdot yr^{-1}$ (Zender et al., 2003; 2004; Shao et al., 2011). The high temporal and spatial variability of dust concentrations and the variability in their microphysical and optical properties present a significant challenge to our understanding of how these particles impact the environment (Dubovik et al., 2002). Many measurements worldwide have been made using different approaches, including satellites which can provide global coverage of mineral dust properties. However, the retrievals of particle properties are still affected by large uncertainties (Levy et al., 2013) and the information on mineral dust properties is quite scarce (Formenti et al., 2011).

One of the areas frequently influenced by mineral dust is the Mediterranean Sea region, affected by dust intrusions from the close Sahara Desert or the Middle-East region (Moulin et al., 1998; Israelevich et al., 2012; Gkikas et al., 2013) producing significant perturbations to the shortwave (SW) and the LW radiation balance (di Sarra et al. 2011; Papadimas et al., 2012; Perrone et al., 2012; Meloni et al. 2015~~; Perrone et al., 2012~~) as well as the regional climate (Nabat et al., 2015). The ARE in the Mediterranean region can be responsible for a strong cooling effect both at the surface (or bottom of the atmosphere, BOA) and the top of the atmosphere (TOA). The so-called forcing efficiency (FE), which is defined as the ratio between the ARE and the aerosol optical depth (AOD), for the SW ranges between -150 and -160 $W \cdot m^{-2}$ for solar zenith angles (SZA) in the range 50-60° (di Biagio et al., 2009), being able to reach values larger than 200 $W \cdot m^{-2}$ at the BOA during strong dust events in the Mediterranean region (Gomez-Amo et al., 2011). The LW component accounts for an effect of up to 53% of the SW component and with an opposite sign (di Sarra et al. 2011; Perrone et al., 2012; Meloni et al. 2015).

~~To address these issues, t~~The Aerosol Direct Radiative Impact on the regional climate in the MEDiterranean region (ADRIMED) field campaign within the Chemistry-Aerosol Mediterranean

Experiment (ChArMEx, http://charmex.lsce.ipsl.fr) took place in the Mediterranean region from 11 June to 5 July 2013 (Mallet et al., 2016). It aimed at characterizing the different aerosol particles and their radiative effects using airborne and ground-based measurements collected in the Mediterranean Basin, with special focus on the western region. In particular, two ChArMEx/ADRIMED flights, F30 and F31, from the French ATR 42 environmental research aircraft of SAFIRE (http://www.SAFIRE.fr), took place above southeastern Spain during a Saharan dust episode on 16 and 17 June 2013.

In this paper, we present an analysis of the mineral dust radiative properties during this particular episode taking advantage of the thorough database available. Multiple datasets are used as input in a radiative transfer model (RTM) to evaluate the influence of the different measurements and data processing in the retrieved direct ARE. The model used here is the Global Atmospheric ModEl (GAME; Dubuisson et al., 1996; 2005), which allows calculating both the solar and thermal infrared fluxes. An evaluation against aircraft in situ measurements of radiative fluxes is also presented.

Two main goals are pursued: i) the quantification of the direct ARE for two case studies within a dust transport episode and ii) the evaluation of the model estimates sensitivity to the aerosol input used.

The paper is structured as follows: Section 2 includes a description of both the ground-based and in situ aircraft instrumentation and a short description of the retrieval algorithms used for the present study; Section 3 is devoted to the description of GAME and the input datasets used here and results are presented in Section 4; finally, a short summary and concluding remarks are included in Section 5.

2 Instruments and data

2.1 Ground-based measurements

Ground-based measurements used in this work were carried out at the Andalusian Institute for Earth System Research (IISTA-CEAMA) of the University of Granada, Spain (37.16º N, 3.61º W, 680 m a.s.l.) by the Atmospheric Physics Group of the University of Granada (GFAT-UGR). This experimental site is located in the western Mediterranean basin, near the African continent (~200 km). Therefore, long-range transport of mineral dust particles from North Africa is a main source of natural atmospheric aerosol in the region (e.g. Lyamani et al., 2005; Valenzuela et al., 2012). The station is also affected by long-range

transported smoke (Ortiz-Amezcua et al., 2017) and fresh smoke from nearby biomass burning (Alados-Arboledas et al., 2011). Anthropogenic sources such as pollution from Europe, the Iberian Peninsula and the Mediterranean Sea (Pérez-Ramírez et al., 2016) also affect the station. Local sources are mainly road traffic and central heating systems (Titos et al., 2017).

IISTA-CEAMA station is equipped with a CE-318-4 (*Cimel Electronique*) sun/sky photometer which belongs to the AERONET network (Holben et al., 1998). This instrument makes direct solar irradiance measurements, used to derive aerosol optical depth (AOD), and sky radiance measurements both at least at the following nominal wavelengths (λ): 440, 670, 870 and 1020 nm. The AOD product provided by AERONET have an uncertainty of ±0.01 for $\lambda > 440$ nm and of ±0.02 for $\lambda < 440$ nm (Holben et al., 1998; Eck et al., 1999). AERONET also provides aerosol optical and microphysical properties such as columnar particle size distribution (PSD), real and imaginary parts of the refractive indices (RRI and IRI, respectively), asymmetry factor (*g*) and single scattering albedo (SSA), using the AOD and sky radiance values in an inversion algorithm (Dubovik and King, 2000; Dubovik et al., 2006). For the present study, AERONET Version 2 Level 1.5 (Level 2.0 when available) data are used. The uncertainty in the retrieval of SSA is ±0.03 for high aerosol load ($AOD_{440} > 0.4$) and solar zenith angle > 50º; while for measurements with low aerosol load ($AOD_{440} < 0.2$), the retrieval accuracy of SSA drops down to 0.02–0.07 (Dubovik and King, 2000). For high aerosol load and solar zenith angle > 50°, errors are about 30%–50% for the IRI. For particles in the size range $0.1 < r < 7$ μm (being r the aerosol radius), errors in PSD retrievals are around 10–35%, while for sizes lower than 1 μm and higher than 7 μm retrieval errors rise up to 80–100%. The inversion code provides additional variables such as the volume concentration, effective radius, r_{eff}, and geometric standard deviation of the equivalent lognormal distribution, σ, for fine and coarse modes of the retrieved PSD which will be used in the current study.

The multi-wavelength aerosol Raman lidar MULHACEN, based on a customized version of LR331D400 (Raymetrics S.A.), is operated at Granada station as part of EARLINET/ACTRIS (European Aerosol Research Lidar Network / Aerosols, Clouds, and Trace Gases Research Infrastructure Network; https://www.actris.eu/default.aspx; Pappalardo et al., 2014) since April 2005. The system has a monostatic biaxial configuration, which usually requires an overlap correction to minimize the incomplete overlap effect (Navas-Guzmán et al., 2011). The system emits vertically to the zenith by means of a pulsed

Nd:YAG laser with 2nd- and 3rd-harmonic generators, that emits simultaneously at 1064, 532 and 355 nm. The receiving system consists of several detectors, which can split the radiation according to the three elastic channels at 355, 532 (parallel- and perpendicular-polarized; Bravo-Aranda et al., 2013), and at 1064 nm; two nitrogen Raman channels at 387 and 607 nm; and a water vapor Raman channel at 408 nm (Navas-Guzmán et al., 2014). The aerosol ~~particle~~ backscatter coefficient profiles ($\beta_{aer}(z,\lambda)$, being z the vertical height) obtained from the multi-wavelength lidar were calculated with the Klett-Fernald method (Fernald et al., 1972; Fernald, 1984; Klett, 1981, 1985). For the retrieval of the aerosol extinction coefficient profiles ($\alpha_{aer}(z,\lambda)$), a height-independent lidar ratio (LR) obtained by forcing the ~~spatial integral~~ vertical integration of $\alpha_{aer}(z,\lambda)$ to the AOD from AERONET photometer (Landulfo et al., 2003) was assumed. The assumption of a constant LR introduces uncertainty in $\alpha_{aer}(z,\lambda)$ retrievals, especially when different types of aerosol appear at different layers. In our case, the LR used for the Klett-Fernald retrieval are very similar to those provided by GRASP (see Benavent-Oltra et al., 2017). Considering the different uncertainty sources, total uncertainty in the profiles obtained with Klett-Fernald method is usually 20% for $\beta_{aer}(z,\lambda)$ and 25-30% for $\alpha_{aer}(z,\lambda)$ profiles (Franke et al., 2001).

Additionally, surface temperature and pressure are continuously monitored at IISTA-CEAMA by ~~in~~ a meteorological station located 2 m above the ground. At the same location, the global and diffuse downward radiative fluxes for the SW are continuously measured with a CM11 pyranometer (Kipp & Zonen) and diffuse downward radiative fluxes for the LW are measured with a PIR pyrgeometer (Eppley), being both instruments regularly calibrated at the site (Antón et al., 2012, 2014).

Comentado [MJ1]: Hay que decider si lo quitamos o lo mantenemos

2.2 Airborne measurements

The Safire ATR 42 aircraft performed two overpasses above Granada on June 16 (flight F30) and 17 (flight F31) in 2013 during the ChArMEx/ADRIMED campaign. During F30, the SAFIRE ATR 42 descended performing a spiral trajectory from 14:15 to 14:45 UTC, whereas during flight F31, the aircraft ascended in the early morning (from 07:15 to 07:45 UTC) at around 20 km from Granada station (see Fig. 1 from Benavent-Oltra et al., 2017). Additional flight details can be found in previous studies (Denjean et al., 2016; Mallet et al., 2016; Benavent-oltra et al., 2017; Román et al., 2018).

The airborne instrumentation includes a Scanning Mobility Particle Sizer (SMPS) and an Ultra-High Sensitivity Aerosol Spectrometer (UHSAS), for measuring aerosol number size distribution in the submicron range. The Forward Scattering Spectrometer Probe model 300 (FSSP-300) and the GRIMM OPC (sky-OPC 1.129) were used to measure the optical size distributions in the diameter nominal size range between 0.28 and 20 µm and between 0.3 and 32 µm, respectively. A nephelometer (TSI Inc, model 3563) was used to measure the particle scattering coefficient at 450, 550 and 700 nm, and a Cavity Attenuated Phase Shift (CAPS-PMex, Aerodyne Inc.), was employed to obtain the aerosol extinction coefficient (α_{aer}) at 530 nm. For more details on the aircraft instrumentation see Denjean et al. (2016) and references therein. The PLASMA (Photomètre Léger Aéroporté pour la Surveillance des Masses d'Air) system, which is an airborne sun-tracking photometer, was additionally used to obtain AOD with wide spectral coverage (15 channels between 0.34 – 2.25 µm) with an accuracy of approximately 0.01, as well as the vertical profiles of the aerosol extinction coefficient (Karol et al., 2013; Torres et al., 2017).

Airborne radiative fluxes (F) were measured with Kipp & Zonen CMP22 pyranometers and CGR4 pyrgeometers. Upward and downward SW fluxes ($^{\uparrow}F_{SW}$ and $^{\downarrow}F_{SW}$) were measured in the spectral range 297-3100 nm by two instruments located above and below the aircraft fuselage. The same setup was used for the pyrgeometers, which provided the LW upward and downward radiative fluxes ($^{\uparrow}F_{LW}$ and $^{\downarrow}F_{LW}$) for wavelengths larger than 4 µm. Both pyranometers and pyrgeometers were calibrated in January 2013 and data were corrected for the temperature dependence of the radiometer's sensitivity following Saunders et al. (1992).

~~Downward pyrgeometer measurements~~Radiation measurement data from the aircraft were filtered out for large pitch and roll angles and corrected from the rapid variations of the solar incidence angle around the solar zenith angle due to the aircraft attitude (pitch and roll). This correction also depends on aircraft heading angle and solar position. It should be noted that, beforehand, roll and pitch offsets must be determined (the axis sensor is not necessarily vertical on average during a horizontal leg). Cosine errors were taken into account. Finally, data were corrected from variations of the solar zenith angle (SZA) during the flight to ease the comparison with GAME retrievals. After these various corrections, an estimated uncertainty of ±6 $W \cdot m^{-2}$ is considered to affect the data, taking into account the accuracy of the

calibration and of the acquisition system together with the consistency of airborne measurements (Meloni et al., 2018).

2.3. The GRASP code

The GRASP (Generalized Retrieval of Aerosol and Surface Properties) code (Dubovik et al., 2011, 2014), provides aerosol optical and microphysical properties in the atmosphere by combining the information from a variety of remote sensors (e.g. Kokhanovsky et al., 2015; Espinosa et al., 2017; Torres et al., 2017; Román et al., 2017, 2018; Chen et al., in review). In our case, GRASP was used to invert simultaneously coincident lidar data (range corrected signal, RCS, at 355, 532 and 1064 nm) and sun/sky photometer measurements (AOD and sky radiances both at 440, 675, 870 and 1020 nm) providing a detailed characterization of the aerosol properties, both column-integrated and vertically-resolved. It is worthy to note that this GRASP scheme, based on Lopatin et al. (2013), presents the main advantage that it allows retrieving aerosol optical and microphysical properties for two distinct aerosol modes, namely fine and coarse. The α_{aer}, β_{aer}, SSA (all at 355, 440, 532, 675, 870, 1020 and 1064 nm), and aerosol volume concentration (VC) profiles obtained as output from GRASP will be used as input to GAME in the present study, together with the column-integrated PSD properties (namely r_{eff} and σ for fine and coarse modes). A more in-depth analysis of GRASP output data retrieved using the lidar and sun/sky photometer data at Granada station for the two inversions simultaneous to the aircraft overpasses during flights F30 and F31 during ChArMEx/ADRIMED campaign can be found in Benavent-Oltra et al. (2017).

3. GAME radiative transfer model

3.1. GAME description

The GAME code is widely described by Dubuisson et al. (2004; 2005) and Sicard et al. (2014a). It is a modular RTM that allows calculating upward and downward radiative fluxes at different vertical levels from the ground up to 20 km (100 km) in the SW (LW) spectral range. The solar and thermal infrared fluxes are calculated in two adjustable spectral ranges, which in this study were fixed to match those of the aircraft radiation measurements, namely 297 - 3100 nm for the SW and 4.5 – 40 μm for the LW, by

using the discrete ordinates method (Stamnes et al., 1988). Note that the GAME code has a variable spectral sampling in the SW (depending on the spectral range considered) and a fixed spectral sampling (115 values) in the LW spectral range (Table 1).

[Table 1]

3.2. GAME input data parameterization

The two considered SAFIRE ATR 42 flights, F30 and F31, took place on 16 and 17 June 2013, respectively, simultaneously to ground-based lidar and sun/sky photometer measurements performed at the station. On these days, mineral dust with origin in the Sahara region (southern Morocco near the border with Algeria) reached Granada after ~4 days of travelling, according to back-trajectories analysis (not shown) and the results presented in Denjean et al. (2016). A homogenous dust layer reaching up to 5 km agl was observed on June 16, whereas on June 17 the dust layer was decoupled from the boundary layer and located between 2 and 4.5 km agl (Benavent-Oltra et al., 2017). A similar structure was observed also above Minorca (Renard et al., 2018), which is an indicator of the horizontal extension of the dust event. On June 16, the F30 ~~profile~~ flight above Granada site took place between 14:15 and 14:45 UTC ~~(averaged SZA=31.49º)~~ in coincidence with the lidar measurements. The corresponding SZA at 14:30UTC was 31.49º. The sun/sky photometer microphysics data were not available till 16:22 UTC, even though the retrieved AOD and its spectral dependence (represented by the Angström exponent) were very stable between the time of the lidar measurements and the time of the sun/sky photometer inversion. On June 17, the F31 ~~profile~~ flight occurred in the early morning (07:15 to 07:45 UTC, with SZA=~~averaged SZA=~~61.93º at 07:30UTC), and simultaneous lidar and sun/sky photometer were available. Unfortunately, the airborne vertical profile of extinction by the CAPS measurements was not available during this second flight. Clouds were detected by the lidar on June 17 after 15:00 UTC. Furthermore, the ground-based pyranometer and pyrgeometer data indicate cloud contamination in the radiation data much earlier (around 09:00 UTC), preventing also satellite retrievals in the region.

A summary of the experimental data used as input for GAME calculations during these two case studies is presented in Table 2. This input includes namely surface parameters and atmospheric profiles of meteorological variables, main gases concentrations and aerosol properties. The aerosol properties used in the present study are parameterized using three different datasets, based on the different instrumentation

and retrievals available, i.e. Dataset 1 (DS1), Dataset 2 (DS2) and Dataset 3 (DS3). A more detailed description of the different parameters is provided next.

[Table 2]

3.2.1. Surface parameters and profiles of meteorological variables

The surface parameters required for GAME are the surface albedo (*alb*(λ)) and land-surface temperature (LST). The *alb*(λ) for the SW range is obtained from the sun/sky photometer data using the AERONET retrieval at 440, 675, 880 and 1020 nm, and for the LW from the integrated emissivity between 4 and 100 μm provided by the Single Scanner Footprint (SSF) Level2 products of the CERES (Clouds and the Earth's Radiant Energy System; (http://ceres.larc.nasa.gov/) instrument (Table ~~Table~~ 3). LST values are obtained from MODIS (Moderate Resolution Imaging Spectroradiometer) 1-km daily level-3 data (Wan et al., 2014) on June 16. Unfortunately, on June 17 MODIS data were not available due to the presence of clouds and the local surface temperature was ~~estimated~~ obtained from temperature measurements at Granada site, where the meteorological station is located at 2 m above the ground. LST and *alb*(λ) values used for the two analyzed cases are included in Table 3.

Con formato: Fuente: 12 pto

[Table 3]

Figure 1 shows the pressure (P), temperature (T), and relative humidity (RH) profiles obtained from the SAFIRE ATR 42 measurements. Data from the meteorological station located at IISTA-CEAMA are used to complete these profiles at the surface level, whereas at altitudes above the aircraft flight, a scaled US standard atmosphere is used for completion. The concentration profiles of the main absorbing gases (O_3, CH_4, N_2O, CO and CO_2) are also taken from the US standard atmosphere, while for the gaseous absorption coefficients the HITRAN database is used (as in Sicard et al., 2014a; 2014b).

[Figure 1]

3.2.2. Aerosol parameterization

As for the aerosol parameterization, $\alpha_{aer}(\lambda,z)$, SSA(λ,z) and $g(\lambda,z)$ are required as GAME input data (Table 2). For the SW wavelengths, these properties can be obtained from the measurements performed with the instrumentation available during the campaign; namely the lidar, the sun/sky photometer and the in situ instrumentation onboard the aircraft. On the other hand, direct measurements of the aerosol properties in

the LW are not so straightforward and thus scarce. Hence, the aerosol LW radiative properties are calculated by a Mie code included as a module in GAME. According to Yang et al. (2007), the dust particles non-sphericity effect at the thermal infrared wavelengths is not significant on the LW direct ARE, thus the shape of the mineral dust can be assumed as spherical for the Mie code retrievals introducing negligible uncertainties.

For the SW simulations, we run GAME using three different aerosol input datasets, i.e. DS1, DS2 and DS3 (Table 2), in order to evaluate their influence on the ARE calculations. DS1 relies on a parameterization based on the advanced post-processing GRASP code, which combines lidar and sun/sky photometer data to retrieve aerosol optical and microphysical properties profiles; DS2 relies on Klett-Fernald lidar inversions and AERONET products and corresponds to a reference parameterization (easily reproducible at any station equipped with a single- or multi-wavelength lidar and an AERONET sun/sky photometer and without the need of an advanced post-processing algorithm); and DS3 relies on in situ airborne measurements and corresponds to an alternative parameterization to DS1 and DS2.

Figure 2~~Figure 2~~ shows α_{aer} profiles on June 16 (top) and 17 (bottom) obtained using the three different approaches. For DS1 (Figure 2~~Figure 2~~a and d), α_{aer} profiles at seven different wavelengths obtained with GRASP are used as input data in GAME. In DS2 (Figure 2~~Figure 2~~b and 3e), the α_{aer} profiles are obtained from the lidar data using Klett-Fernald retrievals and adjusting the lidar ratio to the AERONET retrieved AODs, as mentioned in Section 2.1. Finally, for DS3 the α_{aer} values are obtained from the aircraft in situ measurements (CAPS and PLASMA data on June 16 and PLASMA on June 17). A detailed analysis and discussion on the comparison between α_{aer} profiles provided by the aircraft measurements, GRASP and the lidar system at Granada is already included in Benavent-Oltra et al. (2017). In general, the lidar, GRASP and the CAPS data are in accordance, observing the same aerosol layers and similar values, with ~~discrepancies~~ differences within 20%. GRASP slightly overestimates CAPS data by 3 Mm^{-1} on average, whereas the differences with PLASMA are larger, reaching a 30% (or 11 Mm^{-1}). In the case of the Klett-Fernald retrieval, values are lower than those retrieved with GRASP by up to 19%. Considering that the uncertainty in α_{aer} is around 30% for both GRASP and the Klett-Fernald retrieval and 3% for the CAPS data, this discrepancy is well below the combined uncertainty of the different datasets. ~~Discrepancies~~ Differences in the α_{aer} profiles translate into differences in the

Con formato: Fuente: 12 pto

Con formato: Fuente: 12 pto

Con formato: Fuente: 12 pto

integrated extinction and, hence, in differences in the AOD values used as input in the radiative fluxes retrievals. The AOD values presented here (included in Table 4) are obtained by integrating the α_{aer} profiles~~, interpolated~~ at 550 nm~~,~~ from the surface up to the top of the aerosol layer (4.3 km on June 16 and 4.7 km on June 17). In GRASP retrieved α_{aer} profiles, values above the top of the aerosol layer are slightly larger than zero, thus the approach used here to calculate the AOD leads to lower values compared to the column-integrated AOD provided by the sun-photometer. Differences among the three datasets are more noticeable on June 16, when the AOD for DS1 is 0.05 lower than for DS2 and DS3, whereas on June 17 the maximum difference is 0.03, obtained between DS1 and DS2. The AOD values at 550 nm reveal that GRASP input data (DS1) and in a lesser extent the aircraft in situ data (DS3) underestimate the aerosol load in the analyzed dust layer compared to AERONET (DS2) due to the differences in the retrieval techniques, e.g. whereas AERONET provides integrated AOD for the whole column, low α_{aer} values above the aerosol layer are neglected for the AOD calculations in DS1 and DS3.

[Figure 2]

[Table 4]

Figure 3 presents the SSA values retrieved by GRASP algorithm, used as input for GAME in DS1, on June 16 (F30, Figure 3a) and 17 (F31, Figure 3b). The mean SSA at 440 nm is equal to 0.92 on June 15, whereas on June 17 is 0.85. ~~-On~~On June 17 the SSA profiles present lower values and more variation with height than on June 16; the lower SSA values indicate the presence of more absorbing particles on June 17. The vertical variation on June 17 is associated to the presence of two different layers, whereas a more homogeneous dust layer is observed on June 16. - For DS2, the SSA are taken from AERONET columnar values and assumed to be constant with height (Figure 4a). The SSA at 440 nm was 0.89 and 0.83 on June 16 and 17 respectively, so~~A~~ , as already observed in Figure 3, SSA values are lower on June 17 due to the intrusion of more absorbing particles. For DS3, SSA values at 530 nm are obtained from the nephelometer and the CAPS or PLASMA onboard the ATR. In order to reduce the uncertainty of the measured data, only averaged values for the column will be considered, being 0.88 and 0.83 on June 16 and June 17 (Figure 4). Therefore, differences of up to 0.04 and 0.02 are observed on June 16 and 17 respectively among the SSA values obtained with the three datasets. Despite these difference ~~between the aircraft and AERONET SSA values~~, the retrieved SSA values obtained here are within the range of typical values for dust aerosols (Dubovik et al., 2002; Lopatin et al., 2013) and ~~discrepancies~~ differences are still within the uncertainty limits, which range between 0.02 and 0.07 depending on the aerosol load for AERONET data (Dubovik et al., 2000) and is 0.04 for the aircraft values. In the case of g values, the same data are used for the three aerosol input datasets. Multispectral values of g are taken from AERONET columnar values and assumed to be constant with height (Figure 4b).

[Figure 3]

[Figure 4]

Con formato: No ajustar espacio entre texto latino y asiático, No ajustar espacio entre texto asiático y números

Summing up, for the SW aerosol parametrization in GAME three datasets are tested. In DS1, GRASP provided spectral profiles at 7 wavelengths of the aerosol extinction and SSA are used. In DS2, the Klett retrieved extinction profiles at 3 wavelengths are used together with the AERONET SSA columnar values at 4 wavelengths, which are assumed to be constant with height. For DS3, one extinction profile at 550 nm and a column-averaged monospectral value of the SSA from the airborne measurements are considered. In the three cases, the column-integrated AERONET asymmetry parameter at 4 wavelengths is assumed to be constant with height and used as input.

For the LW calculations, the Mie code is used to obtain $\alpha_{aer}(\lambda,z)$, SSA(λ,z) and g(λ,z) from the information on the aerosol PSD, complex refractive index (RI) and density, following a similar approach to that used in previous studies (Meloni et al., 2015; 2018; Peris-Ferrús et al., 2017). A summary of the aerosol parameters used in the Mie calculations is included in Table 5. Three different datasets are also used for the aerosol parameterization in the LW calculations. In this case, the sensitivity of the model to the PSD used is tested. A similar scheme to that presented for the SW is used, where DS1 relies on GRASP retrievals, DS2 on AERONET products and DS3 relies on in situ airborne measurements.

[Table 5]

The spectral real and imaginary parts of the RI of mineral dust in the LW are obtained from Di Biagio et al. (2017), using the Morocco source, and assumed constant with height. The analysis by Di Biagio et al. (2017) only covers the spectral range 3-16 μm, so an extrapolation assuming the spectral dependence presented in Krekov (1993) for shorter and longer wavelengths is performed. This assumption is not exempt of uncertainty, since the refractive index present a certain variability associated to the different nature of mineral dust properties. For example, the use of the refractive index provided for the Algerian and Mauritanian sources from Di Biagio et al., (2017) leads to variations in the ARF of 0.8 and 0.3 $W \cdot m^{-2}$ at the BOA and the TOA respectively. Additionally, vertical variations of the refractive index are also a source of uncertainty in the obtained radiative fluxes. The mineral dust particle density is assumed to be 2.6 $g \cdot cm^{-3}$ (Hess et al., 1998). Regarding the PSD, three parameters (namely the effective radii, r_{eff}, standard deviation, σ, and the numeric concentrations, *N*) for fine and coarse modes are used. The fine mode comprises particles within the diameter range 0.1–1 μm, whereas for the coarse mode the range 1-

30 µm is considered. In the case of DS1, *N* values are obtained from the volume concentration profiles provided by GRASP assuming spherical particles in the range between 0.05 and 15 µm radii (Figure 5~~Figure 5~~). Values of r_{eff} and σ provided by GRASP (Table 4) are column-integrated and thus assumed to be constant with height. This is the case also for DS2, in which the PSD parameters are column-integrated values provided by the AERONET retrieval in Granada (see Table 4).

[Figure 5]

For DS3, the volume concentration (or the equivalent *N*), *r* and σ profiles for the fine and coarse modes (Figure 5~~Figure 5~~) are calculated from the data provided by the aircraft in situ measurements in the range between 0.02 and 40 µm diameter. Benavent-Oltra et al. (2017) found a general good accordance between the volume concentration profiles measured by the instrumentation onboard the SAFIRE ATR 42 and retrieved with GRASP, with ~~discrepancies~~differences in the total volume concentration profiles for the dust layers lower than 8 $\mu m^{-3} \cdot cm^{-2}$ (20%), which fall within the combined uncertainty. Nonetheless differences are still noticeable, especially in the fine mode. On June 17, GRASP overestimates the aircraft measurements for the fine mode and underestimates them for the coarse mode, which in turns results in a quite different fine to coarse concentration ratio for DS1 and DS3. Additionally, a slight shift is observed in the vertical structure of the aerosol layers. Differences are mostly technical, i.e., GRASP retrieval is based on 30-min averaged lidar profiles while the aircraft provide instantaneous measurements, but they can be also partially caused by the discrepancies between the vertical aerosol distribution above Granada (sampled by the lidar) and the concentration measured during the aircraft trajectory as they are not exactly coincident. In addition, for June 16, there is a 2 hours' time difference between the sun/sky photometer retrieval used in GRASP calculations and the airborne measurements which can lead to slight differences in the aerosol properties despite the homogeneity of the dust event during this period. In the following, we quantify the impact these differences may introduce in the calculations of F.

3.2.3. GAME output data

Con formato: Fuente: 12 pto

Con formato: Fuente: 12 pto

As a result of the simulation, GAME provides vertical profiles of radiative fluxes in the shortwave (F_{SW}) and longwave (F_{LW}) spectral ranges. The net flux can be calculated from the obtained profiles for both spectral ranges as:

$$\text{Net } F = {}^{\downarrow}F - {}^{\uparrow}F \qquad \textbf{Equation 1}$$

where the upward and downward arrows are for upward and downward fluxes respectively. From the obtained radiative fluxes profiles, the direct ARE profiles are calculated according to the following equation:

$$ARE = ({}^{\downarrow}F^{w} - {}^{\uparrow}F^{w}) - ({}^{\downarrow}F^{o} - {}^{\uparrow}F^{o}) \qquad \textbf{Equation 2}$$

where F^{w} and F^{o} are the radiative fluxes with and without aerosols, respectively. The direct ARE can be obtained for the SW (ARE_{SW}) and the LW (ARE_{LW}) spectral ranges.

4 Mineral dust effect on shortwave and longwave radiation

4.1. SW radiative fluxes

Figure 6 shows the radiative fluxes profiles for the SW spectral range obtained with GAME using the three different input datasets described in Section 3, as well as the Net F_{SW}. The radiative fluxes measured by the pyranometer onboard the SAFIRE ATR 42 are also included in the figure. The three GAME simulations show similar values with ~~discrepancies~~ differences below 8 $W \cdot m^{-2}$ on average, which represents less than 1% variation. The differences in the obtained fluxes are mostly due to the differences in the aerosol load considered depending on the inputs. Even though the ~~discrepancies~~ differences in the AOD ~~are within the uncertainty considered for~~among the different datasets are small (lower than 0.05), they can lead to differences in F_{SW} and ultimately in the ARE_{SW}. In order to quantify these differences, we perfomed a sensitivity test by varying the AOD while the other parameters were kept constant. We observed a maximum variation in the F_{SW} of 6.5 $W \cdot m^{-2}$ (0.7%) at the surface, decreasing with height, for changes in the AOD of up to 0.05, which is the difference we observe between the AOD for DS2 and DS1 on June 16. This result partly explains the differences among the three datasets. ~~The larger AOD assumed for DS2 on both days (see Table 4 and Figure 2), causes the ${}^{\downarrow}F_{SW}$ to be slightly lower compared to DS1. For DS3 we can also observe the effect of the SSA values used, which are relatively smaller~~

~~compared to those measured by AERONET (see Figure 4), and lead to lower values of the radiative fluxes, despite the AOD being larger than for DS1.~~ In addition, a sensitivity test performed by varying exclusively the SSA indicates that more absorbing particles are related to less $^{\downarrow}F_{SW}$ at the surface, namely a variation of 1% is observed at the BOA for a decrease in the SSA of 0.03. The influence of the SSA decreases with height being negligible at the TOA. For the $^{\uparrow}F_{SW}$, a decrease of 0.8% is observed at the BOA if more absorbing particles are present, but in this case the influence at the TOA is larger (2.2%). In our case, ~~T~~the larger AOD assumed for DS2 on both days (see Table 4 and Figure 2), causes the $^{\downarrow}F_{SW}$ to be slightly lower compared to DS1. For DS3 the AOD is also lower than for DS2, but ~~we can also observe the effect of the~~the SSA values used, which are relatively smaller compared to those measured by AERONET (see Figure 4), ~~and~~ lead to lower values of the radiative fluxes than for DS2. ~~, despite the AOD being larger than for DS1.~~

The evaluation against the aircraft measurements ~~is limited to the altitude range below 5 km but this does not present a limitation since most of aerosols are below that height (see Figure 2 and Figure 5).~~shows l ~~L~~arger ~~discrepancies~~ differences ~~are observed~~ for altitudes below 2.5 km (~860 mbar) on June 16, whereas a better agreement is found above. ~~This is somehow expected due to the distance between the flight trajectory and the ground-based station (~20 km) and the influence of the boundary layer in the lower altitude range.~~ On June 17, no $^{\uparrow}F_{SW}$ aircraft data are available ~~above~~ below 2 km. Relative ~~D~~ddifferences between the model and the aircraft measured data (calculated as $(F_{GAME}-F_{aircraft})/F_{aircraft}$) are well below 7%, being the largest discrepancies observed for the $^{\downarrow}F_{SW}$. D~~iscrepancie~~fferences between the three GAME outputs and the aircraft pyranometer are lower than 5% for the Net F_{SW} on both days. Considering the very different approaches followed by the model and the direct measurements by the airborne pyranometer (i. e. vertical resolution, temporal sampling and data acquisition and processing), together with the uncertainty of the pyranometer (6 $W \cdot m^{-2}$) and the estimated uncertainty of the model outputs, which can be as large as 19 $W \cdot m^{-2}$)~~the differences are quite insignificant~~these differences are quite reasonable. ~~and a~~A conclusive result on which input dataset provides a better performance is unlikely because of the similar results obtained with the three datasets.

[Figure 6]

Con formato: Sangría: Primera línea: 0 cm

Con formato: Subíndice

Con formato: Subíndice

Con formato: Subíndice

The values at the surface (or bottom of the atmosphere, BOA) and at the top of the atmosphere (TOA) for the different radiative fluxes can be also evaluated against different instruments: measurements for the $^{\downarrow}F_{SW}$ at the surface are available from the CM11 pyranometer located at the ground-station in Granada ~~; CERES provides data of the $^{\uparrow}F_{SW}$ at the TOA;~~ and AERONET provides values of the $^{\downarrow}F_{SW}$ and $^{\uparrow}F_{SW}$ at both the BOA and the TOA. The time series for these measurements corresponding to 16-17 June and the results obtained with GAME for the different datasets are shown in Figure 7. ~~Agreement is found between AERONET, the CM11 and the three GAME simulations on June 17 at the BOA. On June 16, when the radiation presents larger values, a 6% overestimation is observed in GAME (around 60 W·m^{-2}) compared to the pyranometer. A direct comparison with AERONET values is not possible on June 16 since GAME retrievals and the sun/sky photometer measurements are ~2 hours away.~~

In order to compare GAME results with AERONET data, we have performed additional simulations for the time of the closest AERONET measurement on June 16 (at 16:22UTC), assuming that the aerosol parameterization is constant with time between the flight time and the photometer measurement. $^{\downarrow}F_{SW}$ values at the surface obtained with GAME are 564.8, 551.8 and 547.0 W·m^{-2} for DS1, DS2 and DS3 respectively, very similar to the 531.4 W·m^{-2} provided by AERONET. On June 17, GAME simulations at 07:40UTC (instead of 07:30UTC, which is the time of the flight), provide $^{\downarrow}F_{SW}$ at the surface of 466.3, 468.3 and 456.4 W·m^{-2}, very close to the AERONET value of 463.7 W·m^{-2}. An evaluation of the CM11 pyranometer data at the surface against AERONET $^{\downarrow}F_{SW}$ using the simultaneous data available on June 16 and 17 (6 pairs of data) shows large differences (up to 130 W·m^{-2} in one of the cases), which indicates that the CM11 are affected by a large uncertainty due to problems with the maintenance and operation of the instrument during the campaign. Therefore, a quantitative comparison is not reliable.

Comentado [MJ2]: Lo quitamos?

At the TOA, the $^{\uparrow}F_{SW}$ between GAME and AERONET are in quite good agreement on both days. On June ~~17~~16, ~~when measurements are coincident~~ the $^{\uparrow}F_{SW}$ obtained with GAME simulations is equal to 152.0, 153.0 and 148.5 W·m^{-2} and with AERONET is equal to 146.2 W·m^{-2}. On June 17, the obtained values with GAME are 133.6, 136.6 and 130.9 W·m^{-2} for DS1, DS2 and DS3 and 131.6 W·m^{-2} for AERONET. ~~In the case of CERES, only a qualitative comparison is possible since no simultaneous and co-located data are available for the analyzed dates. CERES overpasses Southern Spain during daytime~~

~~at 10 – 11 UTC in summer while the flights were at 14:30UTC and 07:30UTC on June 16 and 17, respectively, so that both datasets are not simultaneous. As an example, Sicard et al. (2016) compared AERONET to CERES F_{SW} at the TOA, and allowed a time difference between AERONET and CERES within ±15 min for validation purposes. Since no closest data were available on 16 and 17 June, we selected satellite overpasses within 600 km from Granada, thus differences are expected. It is also worth noticing that, as reported by Sicard et al. (2016), CERES fluxes present two major sources of artificially added flux: 1) the presence of clouds in the pixel, which is very likely here on 17 June, and 2) possible sun glints. In both cases the result is an increase of CERES upward fluxes at the TOA. In addition, while the spectral range of GAME was set to the aircraft SW band (0.297 – 3.1 μm), the shortwave window of CERES is 0 – 5 μm. Thus, even though data are consistent, the comparison of CERES with GAME simulations cannot be considered as conclusive.~~

[Figure 7]

The ARE_{SW} profiles, calculated by using Eq. 2 and GAME simulations for the three input datasets are shown in Figure 8, together with the simultaneous values provided by AERONET on 17 June at the BOA and TOA. Comparing the three GAME simulations, we can see that the low discrepancies in the F profiles from Figure 6 lead to variations in the ARE_{SW} of 10-27% (3-10 $W \cdot m^{-2}$) over the averaged profile depending on the input dataset used. The variations in the ARE_{SW} are tightly connected to ~~discrepancies~~ differences in the AOD considered as input in the model, as already observed in previous studies (Sicard et al., 2014a; Lolli et al., 2018; Meloni et al., 2018). The SSA and the vertical distribution of the aerosol also plays an important role, as observed for DS3, which shows a profile quite different from DS2 despite the AOD being quite close for both datasets and in agreement with previous studies (Guan et al., 2010; Gomez-Amo et al., 2011).~~.~~

Differences are also observed when comparing ARE_{SW} values obtained from GAME to those retrieved by AERONET. Contrary to GAME simulations, AERONET does not consider the vertical distribution of the aerosols when calculating the ARE_{SW}, and the definition of the ARE_{SW} at the BOA ($^{BOA}ARE_{SW}$) is slightly different. Indeed, AERONET $^{BOA}ARE_{SW}$ is calculated as the difference between the downward fluxes with and without aerosols, the difference between the upward fluxes (reflected by the Earth) being neglected. Considering this, we can correct the $^{BOA}ARE_{SW}$ provided by AERONET

Con formato: Sangría: Primera línea: 0 cm

Con formato: Superíndice

multiplying by a factor (1- *alb*(λ)). The corrected $^{BOA}ARE_{SW}$ value on 17 June is thus -31.9 W·m^{-2}, which is within the range of values provided by GAME at the surface. All discrepancies observed here are mostly intrinsic to the different techniques used for the acquisition of the data and the retrieval algorithms. The effect of the data processing has also been observed in previous studies (Lolli et al., 2018).

The sensitivity tests performed reveal that an increase in the AOD of 0.05 can lead to a stronger effect of the ARE both at the BOA (up to 6.7 W·m^{-2}) and the TOA (up to 2.5 W·m^{-2}), and more absorbing particles (decrease in the SSA of 0.03) lead to more ARE at the BOA and less at the TOA (4 and 2 W·m^{-2} in absolute terms, respectively). Therefore, the differences among the datasets are within the estimated uncertainty.

The ARE_{SW} values obtained at the BOA and TOA for the three datasets and the averaged value, as well as the FE, -are included in Table ~~Table~~ 6. Both at the BOA and TOA, the ARE_{SW} has a cooling effect, as expected for mineral dust in this region according to values obtained in the literature (e.g. Sicard et al. 2014a, Mallet et al., 2016). The values of the ARE and the FE are highly dependent on the SZA and a straightforward comparison with previous studies is not simple. Nonetheless, the values obtained for this case are ~~very similar to the regional summer mean value obtained by Papadimas et al., (2012) at the surface (-26.5 W·m^{-2}) and the TOA (-6.3 W·m^{-2}) and~~ are within the range of previous values observed in the western Mediterranean region for similar values of SZA ~~, which varied from −93.1 to −0.5 W·m^{-2} at the BOA and -34.5 to +8.5 W·m^{-2} at the TOA~~ (e.g. Gomez-Amo et al., 2011; Sicard et al., 2014a,b; Barragan et al., 2017).

[Table 6]

[Figure 8]

4.2. LW radiative fluxes

Figure 9~~Figure 9~~ shows F_{LW} calculated with GAME after obtaining the aerosol properties in the LW spectral range from Mie calculations ~~from~~ for the three mentioned datasets (see Section 3.2.2). F_{LW} measured by pyrgeometers located onboard the ATR is also shown.

In general, differences in the F_{LW} are always lower than 6% (lower than 10 W·m^{-2} on average), with the airborne values being overestimated by the model on 16 June and underestimated on 17 June.

Con formato: Normal

Con formato: Fuente: 12 pto

Con formato: Fuente: 12 pto

On this latter day, larger differences are observed on the Net F_{LW} compared to 16 June, which might be explained by the inaccurate value of LST used due to the lack of precise data. ~~assumed profiles of gases such as CO_2, O_3 or water vapor, or the uncertainty in the LST. The $^{\downarrow}F_{LW}$ is highly dependent on the LST and, unfortunately, no LST data from MODIS were available on 17 June.~~A sensitivity test performed by increasing the air surface temperature measured at the meteorological station up to 5K indicates that the $^{\uparrow}F_{LW}$ increases its value up to 30 $W \cdot m^{-2}$ at the surface, and around 10 $W \cdot m^{-2}$ from 1 km onwards which is non-negligible. This would lead to an overestimation of the aircraft measured values, but still within a 6% difference. This highlights the need for accurate LST measurements for radiation simulations in the LW spectral range. ~~A likely slight contamination by clouds on 17 June on the aircraft measurements may also partially explain this larger difference on 17 June. On the other hand, the influence of the aerosol particles in the F_{LW} is too weak to fully explain the observed differences, as the aerosol load was low (AOD at 550 nm ranging between 0.18 and 0.23).~~ Additionally, a sensitivity test performed by assuming a 10% uncertainty in the PSD parameters (r_{eff}, N and σ) leads to an estimated uncertainty of the F_{LW} retrieved by GAME of around 1.2 $W \cdot m^{-2}$. As stated before, the assumption of the refractive index can also introduce variations as large as 0.8 $W \cdot m^{-2}$. Considering the uncertainty of the pyrgeometer and the fact that the aircraft and the model present different vertical resolutions and time samplings and the uncertainties due to the use of the standard atmosphere or the parameterization of the surface properties the obtained differences are not significant.

[Figure 9]

A comparison of GAME results against the observations from ground-based pyrgeometer at Granada station ~~and against CERES values obtained at the TOA~~ is included in Figure 10. At the BOA, the ~~diffuse~~ longwave radiation measured by the pyrgeometer is in quite good agreement with GAME calculations on 16 June, with differences within 1 $W \cdot m^{-2}$. However, GAME overestimates the pyrgeometer data by 5 $W \cdot m^{-2}$ (1.3%) on 17 June. These ~~larger~~ difference on June 17, even though larger than on June 16, is still within the uncertainty limits. ~~discrepancies might be related either to the likely cloud contamination, not accounted for in the model but affecting the pyrgeometer measurements, or to the selection of the LST values. At the TOA, GAME values are slightly larger than those observed by CERES. As for the SW, CERES closest data are around 2 hours and 600 km away from the measurement~~

Con formato: Superíndice
Con formato: Superíndice
Con formato: Subíndice
Con formato: Superíndice

~~site, so only a qualitative comparison is possible. Due to the strong dependency of $^{\downarrow}F_{LW}$ to LST, the large variability in the satellite data and the difference in the horizontal coverage, differences of the order of 10 W·m^{-2} observed on 16 June are considered reasonable. On 17 June, differences between GAME and the closest in time CERES values are of the order of 50 W·m^{-2}, as a result of the likely undetected cloud contamination in the satellite data.~~

[Figure 10]

As for the ARE_{LW}, Figure 11 shows the profiles obtained with GAME using the three datasets as inputs. Values at the BOA and TOA for each dataset and the average values are included in Table ~~Table~~ 7. Opposite to the SW, the ARE_{LW} produces a heating effect both at the BOA and TOA, with positive values. The slight differences in the F^{LW} in Figure 9~~Figure 9~~ due to the use of different aerosol input datasets lead to variations of up to 2 W·m^{-2} in the $^{BOA}ARE_{LW}$ (ranging from 20 to 26%), which needs to be considered in the interpretation of the results and reduced for a better estimate of the direct ARE. Despite this, values obtained for this dust event (3.2 W·m^{-2} on average for both days) are in agreement with previous studies performed for mineral dust in the infrared region (Sicard et al., 2014a; 2014b; Meloni et al., 2018). It is extremely interesting to look at the differences between the two days in terms of AOD (ΔAOD) and the effective radius for the coarse mode, $r_{e\underline{eff,c}}$, ($\Delta r_{\underline{eff,c}}$) and their implication on the differences in the ARE_{LW} at the BOA ($\Delta^{BOA}ARE_{LW}$). For DS1 ΔAOD ($\Delta r_{\underline{eff,c}}$) is -0.02 (+0.18 μm) which produces a decrease in $^{BOA}ARE_{LW}$ ($\Delta^{BOA}ARE_{LW}$ = -0.5 W·m^{-2}). For DS2 ΔAOD ($\Delta\ r_{\underline{eff,c}}$) is -0.04 (+0.18 μm) which produces a decrease in ^{BOA} ARE_{LW} ($\Delta^{BOA}ARE_{LW}$ = -1.0 W·m^{-2}). If we relate these variations to the sensitivity study of Sicard et al. (2014a), in both cases the expected ARE_{LW} increase due to the increase of the coarse mode radii is counterbalanced by the ARE_{LW} decrease when AOD decreases. Oppositely, for DS3 ΔAOD (Δr_c) is -0.05 (+0.64 μm), producing an increase of $^{BOA}ARE_{LW}$ ($\Delta^{BOA}ARE_{LW}$ = +1.6 W·m^{-2}). Here, the large increase of the coarse mode radius dominates over the AOD decrease. Sicard et al. (2014a) show indeed that the largest positive gradient of ARE_{LW} occurs for median radii ranging from 0.1 to 2.0 μm. For DS3 the increase of $^{BOA}ARE_{LW}$ produced by a positive Δr_c is larger than the decrease of $^{BOA}ARE_{LW}$ that would have produced ΔAOD alone. At the TOA, same trends, but much less marked, are observed.

[Figure 11]

Con formato: Fuente: 12 pto

Con formato: Fuente: 12 pto

[Table 7]

4.3. Total mineral dust radiative effect

The total ARE, including both the SW and LW component, is included in Figure 12~~Figure 12~~ and Table 8. As observed, mineral dust produces a net cooling effect both at the surface and the TOA on both days. Depending on the input dataset used for the aerosol properties, values can change by up to 15 $W \cdot m^{-2}$. On average, the ^{BOA}ARE values are -23.8 ± 8.4 and -29.2 ± 4.0 $W \cdot m^{-2}$, and the ^{TOA}ARE is equal to -2.6 ± 2.2 and -7.0 ± 2.1 $W \cdot m^{-2}$ on 16 and 17 June, respectively. These are 15 and 13% lower than for the SW spectral range, confirming that the LW fraction cannot be neglected. The ARE_{LW} represents approximately 20% of the ARE_{SW} near the surface (except for DS3 on June 16), and reaches up to 50% at higher altitudes where the total ARE is quite low (see 16 June on Figure 12~~Figure 12~~). At higher altitudes low values or the ARE are obtained due to the moderate nature of the analysed dust event, leading to a large variability of the ARE_{LW}/ARE_{SW} and larger values than those observed in previous studies. ~~The highest ARE_{LW}/ARE_{SW} ratio at the TOA is obtained for the lowest values of ARE_{SW} (DS2).~~ Overall these ARE_{LW}/ARE_{SW} ratios are in agreement with those found at the BOA in previous studies for the Mediterranean region, which ranged between 9 and 26% (di Sarra et al. 2011; Perrone and Bergamo 2011; Sicard et al. 2014a; Meloni et al., 2015).

[Figure 12]

[Table 8]

5 Conclusions

A moderate Saharan dust event affecting the western Mediterranean region during the Charmex/ADRIMED campaign on June 2013 was extensively monitored by ground-based and aircraft instrumentation above Granada experimental site. Radiative fluxes and mineral dust ARE both in the solar and infrared spectral ranges are calculated for this event with the RTM GAME. Three different aerosol input datasets, are used by GAME RTM in order to evaluate the impact of different input data in GAME calculations.

For the SW, very low variability with the input aerosol data (less than 1%) is observed for the radiative fluxes. The evaluation of GAME calculated radiative fluxes against the aircraft data reveals

Con formato: Fuente: 12 pto

Con formato: Fuente: 12 pto

differences between the model fluxes and the measurements below 7%, with better agreement at altitudes above the planetary boundary layer. The differences between the retrievals with the three aerosol datasets are quite insignificant, especially taking into account the different approaches followed by the model and the pyranometers. Thus a conclusion on which input dataset provides a better performance is unlikely. The low ~~discrepancies~~ differences between GAME radiative fluxes retrievals lead to variations in the ARE_{SW} of up to 33%, mostly driven by the differences in the aerosol vertical distribution and load, followed by the SSA.

For the LW, the effect of the aerosol in the radiative properties is lower compared to the SW, but certainly non-negligible and of opposite sign. GAME retrievals using the three aerosol datasets reveal differences in the fluxes lower than 2 $W \cdot m^{-2}$ (less than 1%). The comparison with the pyrgeometer data measured at the ATR reveals however differences around 7%. Considering the low influence of the aerosol in the LW radiative fluxes, the influence of the assumed CO_2, O_3 and the used water vapor profiles and LST are needed to fully explain this discrepancy between the aircraft and the simulated profiles.

The total ARE, including both the SW and LW components, confirms that mineral dust produces a cooling effect both at the surface and the TOA, as already reported in the literature. On average, the ARE_{LW} represents a 20% of the ARE_{SW} at the surface, therefore clearly indicating that global model estimates need to consider the complete spectrum to avoid an overestimation on mineral dust cooling effect.

Additionally, it is necessary to be aware of the effects of using different measurement techniques and processing methodologies when calculating aerosol radiative properties. Even though the ~~discrepancies~~ differences observed here when using different aerosol datasets are slight, they still exist and a homogenization of the techniques to feed global models would be beneficial for a better estimate of the ARE and a reduced uncertainty.

Acknowledgements

This work is part of the ChArMEx project supported by CNRS-INSU, ADEME, Météo-France and CEA in the framework of the multidisciplinary program MISTRALS (Mediterranean Integrated Studies aT Regional And Local Scales; http://mistrals-home.org/). Lidar measurements were supported by the

ACTRIS (Aerosols, Clouds, and Trace Gases Research Infrastructure Network) Research Infrastructure Project funded by the European Union's Horizon 2020 research and innovation programme under grant agreement n. 654109. The Barcelona team acknowledges the Spanish Ministry of Economy and Competitivity (project TEC2015-63832-P) and EFRD (European Fund for Regional Development); the Department of Economy and Knowledge of the Catalan autonomous government (grant 2014 SGR 583) and the Unidad de Excelencia Maria de Maeztu (project MDM-2016-0600) financed by the Spanish Agencia Estatal de Investigación. The authors also thank the Spanish Ministry of Sciences, Innovation and Universities (ref. CGL2017-90884-REDT). This work was also supported by the Juan de la Cierva-Formación program (grant FJCI-2015-23904). P. Formenti and C. Denjean acknowledge the support of the French National Research Agency (ANR) through the ADRIMED program (contract ANR-11-BS56-0006). Airborne data was obtained using the aircraft managed by SAFIRE, the French facility for airborne research, an infrastructure of the French National Center for Scientific Research (CNRS), Météo-France and the French National Center for Space Studies (CNES). The authors acknowledge the use of GRASP inversion algorithm (www.grasp-open.com). The authors also kindly acknowledge Philippe Dubuisson (Laboratoire d'Optique Atmosphérique, Université de Lille, France) for the use of GAME model and Rosa Delia García Cabrera for her advice during the preparation of this manuscript.

References

Alados-Arboledas, L., Müller, D., Guerrero-Rascado, J. L., Navas-Guzmán, F., Pérez-Ramírez, D. and Olmo, F. J.: Optical and microphysical properties of fresh biomass burning aerosol retrieved by Raman lidar, and star-and sun-photometry, Geophys. Res. Lett., 38(1), n/a-n/a, doi:10.1029/2010GL045999, 2011.

Antón, M., A. Valenzuela, A. Cazorla, J.E. Gil, J. Fernández-Gálvez, H. Lyamani, I. Foyo-Moreno, F.J. Olmo, L. Alados-Arboledas, Global and diffuse shortwave irradiance during a strong desert dust episode at Granada (Spain), Atmospheric Research, 118, 232-239, doi: 10.1016/j.atmosres.2012.07.007, 2012.

Antón, M., A. Valenzuela, D. Mateos, I. Alados, I. Foyo-Moreno, F.J. Olmo, L. Alados-Arboledas, Longwave aerosol radiative effects during an extreme desert dust event in southeastern Spain, Atmospheric Research, 149, 18-23, doi: 10.1016/j.atmosres.2014.05.022, 2014.

Barragan, R., Sicard, M., Totems, J., Léon, J. F., Dulac, F., Mallet, M., Pelon, J., Alados-Arboledas, L., Amodeo, A., Augustin,

P., Boselli, A., Bravo-Aranda, J. A., Burlizzi, P., Chazette, P., Comerón, A., D'Amico, G., Dubuisson, P., Granados-Muñoz, M. J., Leto, G., Guerrero-Rascado, J. L., Madonna, F., Mona, L., Muñoz-Porcar, C., Pappalardo, G., Perrone, M. R., Pont, V., Rocadenbosch, F., Rodriguez-Gomez, A., Scollo, S., Spinelli, N., Titos, G., Wang, X. and Sanchez, R. Z.: Spatio-temporal monitoring by ground-based and air- and space-borne lidars of a moderate Saharan dust event affecting southern Europe in June 2013 in the framework of the ADRIMED/ChArMEx campaign, Air Qual. Atmos. Heal., 10(3), 261–285, doi:10.1007/s11869-016-0447-7, 2017.

Benavent-oltra, J. A., Román, R., Granados-muñoz, M. J., Pérez-, D., Ortiz-amezcua, P., Denjean, C., Lopatin, A., Lyamani, H., Guerrero-rascado, J. L., Fuertes, D., Dubovik, O., Chaikovsky, A., Olmo, F. J., Mallet, M. and Alados-arboledas, L.: Comparative assessment of GRASP algorithm for a dust event over Granada (Spain) during ChArMEx-ADRIMED 2013 campaign ., Atmos. Meas. Tech., (July), 1–29, 2017.

Boucher, O., Randall, D., Artaxo, P., Bretherton, C., Feingold, G., Forster, P., Kerminen, V., Kondo, Y., Liao, H., Lohmann, U., Rasch, P., Satheesh, S., Sherwood, S., Stevens, B., Zhang, X., Qin, D., Plattner, G., Tignor, M., Allen, S., Boschung, J., Nauels, A., Xia, Y., Bex, V., Midgley, P., Boucher, O. and Randall, D.: Clouds and Aerosols, in Climate Change 2013 - The Physical Science Basis, pp. 571–658., 2013.

Bravo-Aranda, J. A., Navas-Guzmán, F., Guerrero-Rascado, J. L., Pérez-Ramírez, D., Granados-Muñoz, M. J. and Alados-Arboledas, L.: Analysis of lidar depolarization calibration procedure and application to the atmospheric aerosol characterization, Int. J. Remote Sens., 34(9–10), 3543–3560, doi:10.1080/01431161.2012.716546, 2013.

Chen, C., Dubovik, O., Henze, D. K., Lapyonak, T., Chin, M., Ducos, F., Litvinov, P., Huang, X., and Li, L.: Retrieval of Desert Dust and Carbonaceous Aerosol Emissions over Africa from POLDER/PARASOL Products Generated by GRASP Algorithm, Atmos. Chem. Phys. Discuss., https://doi.org/10.5194/acp-2018-35, in review, 2018.

Choobari, O. A., Zawar-Reza, P. and Sturman, A.: The global distribution of mineral dust and its impacts on the climate system: A review, Atmos. Res., 138, 152–165, doi:10.1016/j.atmosres.2013.11.007, 2014.

Denjean, C., Cassola, F., Mazzino, A., Triquet, S., Chevaillier, S., Grand, N., Bourrianne, T., Momboisse, G., Sellegri, K., Schwarzenbock, A., Freney, E., Mallet, M. and Formenti, P.: Size distribution and optical properties of mineral dust aerosols transported in the western Mediterranean, Atmos. Chem. Phys., 16(2), 1081–1104, doi:10.5194/acp-16-1081-2016, 2016.

Di Biagio, C., Formenti, P., Balkanski, Y., Caponi, L., Cazaunau, M., Pangui, E., Journet, E., Nowak, S., Caquineau, S., Andreae O, M., Kandler, K., Saeed, T., Piketh, S., Seibert, D., Williams, E. and Doussin, J. F. C.: Global scale variability of the mineral dust long-wave refractive index: A new dataset of in situ measurements for climate modeling and remote sensing, Atmos. Chem. Phys., 17(3), 1901–1929, doi:10.5194/acp-17-1901-2017, 2017.

di Sarra, A., Di Biagio, C., Meloni, D., Monteleone, F., Pace, G., Pugnaghi, S. and Sferlazzo, D.: Shortwave and longwave radiative effects of the intense Saharan dust event of 25-26 March 2010 at Lampedusa (Mediterranean Sea), J. Geophys. Res. Atmos., 116(D23), n/a-n/a, doi:10.1029/2011JD016238, 2011.

Dubovik, O. and King, M. D.: A flexible inversion algorithm for retrieval of aerosol optical properties from Sun and sky

radiance measurements, J. Geophys. Res. Atmos., 105(D16), 20673–20696, doi:10.1029/2000JD900282, 2000.

Dubovik, O., Holben, B. N., Lapyonok, T., Sinyuk, A., Mishchenko, M. I., Yang, P. and Slutsker, I.: Non-spherical aerosol retrieval method employing light scattering by spheroids, Geophys. Res. Lett., 29(10), 54-1-54–4, doi:10.1029/2001GL014506, 2002.

Dubovik, O., Sinyuk, A., Lapyonok, T., Holben, B. N., Mishchenko, M., Yang, P., Eck, T. F., Volten, H., Muñoz, O., Veihelmann, B., van der Zande, W. J., Leon, J. F., Sorokin, M. and Slutsker, I.: Application of spheroid models to account for aerosol particle nonsphericity in remote sensing of desert dust, J. Geophys. Res. Atmos., 111(11), D11208, doi:10.1029/2005JD006619, 2006.

Dubovik, O., Herman, M., Holdak, A., Lapyonok, T., Tanré, D., Deuzé, J. L., Ducos, F., Sinyuk, A. and Lopatin, A.: Statistically optimized inversion algorithm for enhanced retrieval of aerosol properties from spectral multi-angle polarimetric satellite observations, Atmos. Meas. Tech., 4(5), 975–1018, doi:10.5194/amt-4-975-2011, 2011.

Dubovik, Oleg, et al. "GRASP: a versatile algorithm for characterizing the atmosphere." SPIE Newsroom 25, 2014.

Dubuisson, P., Buriez, J. C. and Fouquart, Y.: High spectral resolution solar radiative transfer in absorbing and scattering media: Application to the satellite simulation, J. Quant. Spectrosc. Radiat. Transf., 55(1), 103–126, doi:10.1016/0022-4073(95)00134-4, 1996.

Dubuisson, P., Dessailly, D., Vesperini, M. and Frouin, R.: Water vapor retrieval over ocean using near-infrared radiometry, J. Geophys. Res. D Atmos., 109(19), doi:10.1029/2004JD004516, 2004.

Dubuisson, P., Giraud, V., Chomette, O., Chepfer, H. and Pelon, J.: Fast radiative transfer modeling for infrared imaging radiometry, J. Quant. Spectrosc. Radiat. Transf., 95(2), 201–220, doi:10.1016/j.jqsrt.2004.09.034, 2005.

Eck, T. F., Holben, B. N., Reid, J. S., Dubovik, O., Smirnov, A., O'Neill, N. T., Slutsker, I. and Kinne, S.: Wavelength dependence of the optical depth of biomass burning, urban, and desert dust aerosols, J. Geophys. Res. Atmos., 104(D24), 31333–31349, doi:10.1029/1999JD900923, 1999.

Espinosa, W.R., Remer, L.A., Dubovik, O., Ziemba, L., Beyersdorf, A., Orozco, D., Schuster, G., Lapyonok, T., Fuertes, D., Martins, J.V. Retrievals of aerosol optical and microphysical properties from imaging polar nephelometer scattering measurements. Atmos. Meas. Tech. 10, 811–824, 2017.

Fernald, F. G.: Analysis of atmospheric lidar observations:, , 23(5) [online] Available from: https://www.osapublishing.org/DirectPDFAccess/12641A7B-F076-A356-C26E134E8E22E7F2_27314/ao-23-5-652.pdf?da=1&id=27314&seq=0&mobile=no (Accessed 26 April 2018), 1984.

Fernald, F. G., Herman, B. M. and Reagan, J. A.: Determination of Aerosol Height Distributions by Lidar, J. Appl. Meteorol., 11(3), 482–489, doi:10.1175/1520-0450(1972)011<0482:DOAHDB>2.0.CO;2, 1972.

Formenti, P., Schütz, L., Balkanski, Y., Desboeufs, K., Ebert, M., Kandler, K., Petzold, A., Scheuvens, D., Weinbruch, S. and Zhang, D.: Recent progress in understanding physical and chemical properties of African and Asian mineral dust, Atmos. Chem. Phys., 11(16), 8231–8256, doi:10.5194/acp-11-8231-2011, 2011.

Franke, K., Ansmann, A., Müller, D., Althausen, D., Wagner, F. and Scheele, R.: One-year observations of particle lidar ratio

over the tropical Indian Ocean with Raman lidar, Geophys. Res. Lett., 28(24), 4559–4562, doi:10.1029/2001GL013671, 2001.

Ginoux, P., Prospero, J. M., Gill, T. E., Hsu, N. C. and Zhao, M.: Global-scale attribution of anthropogenic and natural dust sources and their emission rates based on MODIS Deep Blue aerosol products, Rev. Geophys., 50(3), doi:10.1029/2012RG000388, 2012.

Gkikas, A., Hatzianastassiou, N., Mihalopoulos, N., Katsoulis, V., Kazadzis, S., Pey, J., Querol, X. and Torres, O.: The regime of intense desert dust episodes in the Mediterranean based on contemporary satellite observations and ground measurements, Atmos. Chem. Phys., 13(23), 12135–12154, doi:10.5194/acp-13-12135-2013, 2013.

Gómez-Amo, J.L., A.diSarra, D.Meloni, M.Cacciani, M.P.Utrillas, Sensitivity of shortwave radiative fluxes to the vertical distribution of aerosol single scattering albedo in the presence of a desert dust layer, Atmospheric Environment 44, 2787-2791, 2010.

Gómez-Amo, J.L., V. Pinti, T. Di Iorio, A. di Sarra, D. Meloni, S. Becagli, V. Bellantone, M. Cacciani, D. Fuà, M.R. Perrone, The June 2007 Saharan dust event in the central Mediterranean: Observations and radiative effects in marine, urban, and sub-urban environments, Atmospheric Environment 45, 5385-5393, 2011.

Guan, H., B. Schmid, A. Bucholtz, and R. Bergstrom, Sensitivity of shortwave radiative flux density, forcing, and heating rate to the aerosol vertical profile, Journal of Geophysical Research, 115, D06209, doi:10.1029/2009JD012907, 2010.

Hess, M., Koepke, P. and Schult, I.: Optical Properties of Aerosols and Clouds: The Software Package OPAC, Bull. Am. Meteorol. Soc., 79(5), 831–844, doi:10.1175/1520-0477(1998)079<0831:OPOAAC>2.0.CO;2, 1998.

Holben, B. N., Eck, T. F., Slutsker, I., Tanré, D., Buis, J. P., Setzer, A., Vermote, E., Reagan, J. A., Kaufman, Y. J., Nakajima, T., Lavenu, F., Jankowiak, I. and Smirnov, A.: AERONET - A federated instrument network and data archive for aerosol characterization, Remote Sens. Environ., 66(1), 1–16, doi:10.1016/S0034-4257(98)00031-5, 1998.

Israelevich, P., Ganor, E., Alpert, P., Kishcha, P. and Stupp, A.: Predominant transport paths of Saharan dust over the Mediterranean Sea to Europe, J. Geophys. Res. Atmos., 117(2), n/a-n/a, doi:10.1029/2011JD016482, 2012.

Karol, Y., Tanré, D., Goloub, P., Vervaerde, C., Balois, J. Y., Blarel, L., Podvin, T., Mortier, A. and Chaikovsky, A.: Airborne sun photometer PLASMA: Concept, measurements, comparison of aerosol extinction vertical profile with lidar, Atmos. Meas. Tech., 6(9), 2383–2389, doi:10.5194/amt-6-2383-2013, 2013.

Klett, J. D.: Stable analytical inversion solution for processing lidar returns, Appl. Opt., 20(2), 211, doi:10.1364/AO.20.000211, 1981.

Klett, J. D.: Lidar inversion with variable backscatter/extinction ratios, Appl. Opt., 24(11), 1638, doi:10.1364/AO.24.001638, 1985.

Kokhanovsky, A.A., Davis, A.B., Cairns, B., Dubovik, O., Hasekamp, O.P., Sano, I., Mukai, S., Rozanov, V.V., Litvinov, P., Lapyonok, T., Kolomiets, I.S., Oberemok, Y.A., Savenkov, S., Martin, W., Wasilewski, A., Di Noia, A., Stap, F.A., Rietjens, J., Xu, F., Natraj, V., Duan, M., Cheng, T., Munro, R. Space-based remote sensing of atmospheric aerosols: the multi-angle spectro-polarimetric frontier. Earth Sci. Rev. 145, 85–116, 2015.

Con formato: Inglés (Estados Unidos)

Krekov, G. M.: Models of atmospheric aerosols. In: Jennings SG (ed), Aerosol effects on climate. University of Arizona Press, Tucson, AZ, pp. 9–72, 1993.

Landulfo, E., Papayannis, A., Artaxo, P., Castanho, A. D. A., De Freitas, A. Z., Souza, R. F., Vieira, N. D., Jorge, M. P. M. P., Sánchez-Ccoyllo, O. R. and Moreira, D. S.: Synergetic measurements of aerosols over São Paulo, Brazil using LIDAR, sunphotometer and satellite data during the dry season, Atmos. Chem. Phys., 3(5), 1523–1539, doi:10.5194/acp-3-1523-2003, 2003.

Levy, R. C., Mattoo, S., Munchak, L. A., Remer, L. A., Sayer, A. M., Patadia, F. and Hsu, N. C.: The Collection 6 MODIS aerosol products over land and ocean, Atmos. Meas. Tech., 6(11), 2989–3034, doi:10.5194/amt-6-2989-2013, 2013.

Lolli, S., Madonna, F., Rosoldi, M., Campbell, J. R., Welton, E. J. and Lewis, J. R.: Impact of varying lidar measurement and data processing techniques in evaluating cirrus cloud and aerosol direct radiative effects, Atmos. Meas. Tech., 11, 1639–1651, 2018.

Lopatin, A., Dubovik, O., Chaikovsky, A., Goloub, P., Lapyonok, T., Tanré, D. and Litvinov, P.: Enhancement of aerosol characterization using synergy of lidar and sun-photometer coincident observations: The GARRLiC algorithm, Atmos. Meas. Tech., 6(8), 2065–2088, doi:10.5194/amt-6-2065-2013, 2013.

Lyamani, H., Olmo, F. J. and Alados-Arboledas, L.: Saharan dust outbreak over southeastern Spain as detected by sun photometer, Atmos. Environ., 39(38), 7276–7284, doi:10.1016/j.atmosenv.2005.09.011, 2005.

Mallet, M., Pont, V., Liousse, C., Gomes, L., Pelon, J., Osborne, S., Haywood, J., Roger, J., Dubuisson, P., Mariscal, A., Thouret, V., and Goloub, P.: Aerosol direct radiative forcing over Djougou (northern Benin) during the African Monsoon Multidisciplinary Analysis dry season experiment (Special Observation Period-0), J. Geophys. Res. 113, D00C01, doi:10.1029/2007JD009419, 2008.

Mallet, M., Dulac, F., Formenti, P., Nabat, P., Sciare, J., Roberts, G., Pelon, J., Ancellet, G., Tanré, D., Parol, F., Denjean, C., Brogniez, G., di Sarra, A., Alados-Arboledas, L., Arndt, J., Auriol, F., Blarel, L., Bourrianne, T., Chazette, P., Chevaillier, S., Claeys, M., D'Anna, B., Derimian, Y., Desboeufs, K., Di Iorio, T., Doussin, J.-F., Durand, P., Féron, A., Freney, E., Gaimoz, C., Goloub, P., Gómez-Amo, J. L., Granados-Muñoz, M. J., Grand, N., Hamonou, E., Jankowiak, I., Jeannot, M., Léon, J.-F., Maillé, M., Mailler, S., Meloni, D., Menut, L., Momboisse, G., Nicolas, J., Podvin, T., Pont, V., Rea, G., Renard, J.-B., Roblou, L., Schepanski, K., Schwarzenboeck, A., Sellegri, K., Sicard, M., Solmon, F., Somot, S., Torres, B., Totems, J., Triquet, S., Verdier, N., Verwaerde, C., Waquet, F., Wenger, J., and Zapf, P.: Overview of the Chemistry-Aerosol Mediterranean Experiment/Aerosol Direct Radiative Forcing on the Mediterranean Climate (ChArMEx/ADRIMED) summer 2013 campaign, Atmos. Chem. Phys., 16, 455-504, doi:10.5194/acp-16-455-2016, 2016.

Markowicz, K. M., Flatau, P. J., Vogelmann, A. M., Quinn, P. K. and Welton, E. J.: Clear-sky infrared aerosol radiative forcing at the surface and the top of the atmosphere, Q. J. R. Meteorol. Soc., 129(594 PART A), 2927–2947, doi:10.1256/003590003769682110, 2003.

Meloni, D., Junkermann, W., di Sarra, A., Cacciani, M., De Silvestri, L., Di Iorio, T., Estellés, V., Gómez-Amo, J. L., Pace, G. and Sferlazzo, D. M.: Altitude-resolved shortwave and longwave radiative effects of desert dust in the Mediterranean

during the GAMARFE campaign: Indications of a net daily cooling in the dust layer, J. Geophys. Res., 120(8), 3386–3407, doi:10.1002/2014JD022312, 2015.

Meloni, D., Di Sarra, A., Brogniez, G., Denjean, C., De Silvestri, L., Di Iorio, T., Formenti, P., Gómez-Amo, J. L., Gröbner, J., Kouremeti, N., Liuzzi, G., Mallet, M., Pace, G. and Sferlazzo, D. M.: Determining the infrared radiative effects of Saharan dust: A radiative transfer modelling study based on vertically resolved measurements at Lampedusa, Atmos. Chem. Phys., 18(6), 4377–4401, doi:10.5194/acp-18-4377-2018, 2018.

Moulin, C., Lambert, C.E., Dayan, U., Masson, V, Ramonet, M., Bousquet, P., Legrand, M., Balkanski, Y. J., Guelle, W., Marticorena, B., Bergametti, G., and Dulac, F.: Satellite climatology of African dust transport in the Mediterranean atmosphere, J. Geophys. Res., 103, 13137-13144, doi:10.1029/98JD00171, 1998.

Nabat, P., Somot, S., Mallet, M., Michou, M., Sevault, F., Driouech, F., Meloni, D., di Sarra, A., Di Biagio, C., Formenti, P., Sicard, M., Léon, J.-F., and Bouin, M.-N.: Dust aerosol radiative effects during summer 2012 simulated with a coupled regional aerosol–atmosphere–ocean model over the Mediterranean, Atmos. Chem. Phys., 15, 3303-3326, doi:10.5194/acp-15-3303-2015, 2015

Navas-Guzmán, F., Rascado, J. L. G. and Arboledas, L. A.: Retrieval of the lidar overlap function using Raman signals, Opt. Pura Apl, 44(1), 71–75, 2011.

Navas-Guzmán, F., Fernández-Gálvez, J., Granados-Muñoz, M. J., Guerrero-Rascado, J. L., Bravo-Aranda, J. A. and Alados-Arboledas, L.: Tropospheric water vapour and relative humidity profiles from lidar and microwave radiometry, Atmos. Meas. Tech., 7(5), 1201–1211, doi:10.5194/amt-7-1201-2014, 2014.

Ortiz-Amezcua, P., Luis Guerrero-Rascado, J., Granados-Munõz, M. J., Benavent-Oltra, J. A., Böckmann, C., Samaras, S., Stachlewska, I. S., Janicka, L., Baars, H., Bohlmann, S. and Alados-Arboledas, L.: Microphysical characterization of long-range transported biomass burning particles from North America at three EARLINET stations, Atmos. Chem. Phys., 17(9), 5931–5946, doi:10.5194/acp-17-5931-2017, 2017.

Otto, S., De Reus, M., Trautmann, T., Thomas, A., Wendisch, M. and Borrmann, S.: Atmospheric radiative effects of an in situ measured Saharan dust plume and the role of large particles, Atmos. Chem. Phys., 7(18), 4887–4903, doi:10.5194/acp-7-4887-2007, 2007.

Papadimas, C. D., Hatzianastassiou, N., Matsoukas, C., Kanakidou, M., Mihalopoulos, N. and Vardavas, I.: The direct effect of aerosols on solar radiation over the broader Mediterranean basin, Atmos. Chem. Phys., 12(15), 7165–7185, doi:10.5194/acp-12-7165-2012, 2012.

Pappalardo, G., Amodeo, A., Apituley, A., Comeron, A., Freudenthaler, V., Linné, H., Ansmann, A., Bösenberg, J., D'Amico, G., Mattis, I., Mona, L., Wandinger, U., Amiridis, V., Alados-Arboledas, L., Nicolae, D., and Wiegner, M.: EARLINET: towards an advanced sustainable European aerosol lidar network, Atmos. Meas. Tech., 7, 2389–2409, doi:10.5194/amt-7-389-2014, 2014.

Pérez-Ramírez, D., Lyamani, H., Smirnov, A., O´Neill, N. T., Veselovskii, I., Whiteman, D. N., Olmo, F. J. and Alados-Arboledas, L.: Statistical study of day and night hourly patterns of columnar aerosol properties using sun and star

photometry, in spiedigitallibrary.org, p. 100010K., 2016.

Peris-Ferrús, C., J.L. Gomez-Amo, C. Marcos, M.D. Freile-Aranda, M.P. Utrillas, J.A. Martínez-Lozano, Heating rate profiles and radiative forcing due to a dust storm in the Western Mediterranean using satellite observations, Atmospheric Environment 160, 142-153, 2017.

Perrone, M. R. and Bergamo, A.: Direct radiative forcing during Sahara dust intrusions at a site in the Central Mediterranean: Anthropogenic particle contribution, Atmos. Res., 101(3), 783–798, doi:10.1016/j.atmosres.2011.05.011, 2011.

Perrone, M. R., Tafuro, A. M. and Kinne, S.: Dust layer effects on the atmospheric radiative budget and heating rate profiles, Atmos. Environ., 59, 344–354, doi:10.1016/J.ATMOSENV.2012.06.012, 2012.

Renard, J.-B., Dulac, F., Durand, P., Bourgeois, Q., Denjean, C., Vignelles, D., Couté, B., Jeannot, M., Verdier, N., and Mallet, M.: In situ measurements of desert dust particles above the western Mediterranean Sea with the balloon-borne Light Optical Aerosol Counter/sizer (LOAC) during the ChArMEx campaign of summer 2013, Atmos. Chem. Phys., 18, 3677-3699, https://doi.org/10.5194/acp-18-3677-2018, 2018.

Roger, J., Mallet, M., Dubuisson, P., Cachier, H., Vermote, E.,Dubovik, O., and Despiau, S.: A synergetic approach for estimating the local direct aerosol forcing: Application to an urban zone during the Expérience sur Site pour Contraindre les Modeles de Pollution et de Transport d'Emission (ESCOMPTE) experiment, J. Geophys. Res. 111, d13208, doi:10.1029/2005JD006361, 2006.

Román, R., Torres, B., Fuertes, D., Cachorro, V.E., Dubovik, O., Toledano, C., Cazorla, A., Barreto, A., Bosch, J.L., Lapyonok, T., González, R., Goloub, P., Perrone, M.R., Olmo, F.J. and Alados-Arboledas, L.: Remote sensing of lunar aureole with a sky camera: Adding infomration in the nocturnal retreival of aerosol properties with GRASP code, Remote Sens. Environ., 196, 238-252, http://dx.doi.org/10.1016/j.rse.2017.05.013, 2017.

Román, R., Benavent-Oltra, J.A., Casquero-Vera, J.A., Lopatin, A., Cazorla, A., Lyamani, H., Denjean, C., Fuertes, D., Pérez-Ramírez, D., Torres, B., Toledano, C., Dubovik, O., Cachorro, V.E., de Frutos, A.M., Olmo, F.J. and Alados-Arboledas, L.: Retrieval of aerosol profiles combining sunphotometer and ceilometer measurements in GRASP code, Atmos. Res., 204, 161-177, https://doi.org/10.1016/j.atmosres.2018.01.021, 2018.

Saunders, R. W., Brogniez, G., Buriez, J. C., Meerkotter, R. and Wendling, P.: A comparison of measured and modeled broadband fluxes from aircraft data during the ICE '89 field experiment, J. Atmos. \& Ocean. Technol., 9(4), 391–406, doi:10.1175/1520-0426(1992)009<0391:ACOMAM>2.0.CO;2, 1992.

Shao, Y., Wyrwoll, K. H., Chappell, A., Huang, J., Lin, Z., McTainsh, G. H., Mikami, M., Tanaka, T. Y., Wang, X. and Yoon, S.: Dust cycle: An emerging core theme in Earth system science, Aeolian Res., 2(4), 181–204, doi:10.1016/j.aeolia.2011.02.001, 2011.

Sicard, M., Mallet, M., García-Vizcaíno, D., Comerón, A., Rocadenbosch, F., Dubuisson, P., and Muñoz-Porcar, C.: Intense dust and extremelly fresh biomass burning in Barcelona, Spain: characterization of their optical properties and estimation of their radiative forcing, Environ. Res. Lett., 7, 034016, doi:10.1088/1748-9326/7/3/034016, 2012.

Sicard, M., Bertolín, S., Mallet, M., Dubuisson, P. and Comerón, A.: Estimation of mineral dust long-wave radiative forcing:

Sensitivity study to particle properties and application to real cases in the region of Barcelona, Atmos. Chem. Phys., 14(17), 9213–9231, doi:10.5194/acp-14-9213-2014, 2014a.

Sicard, M., Bertolín, S., Muñoz, C., Rodríguez, A., Rocadenbosch, F. and Comerõn, A.: Separation of aerosol fine- and coarse-mode radiative properties: Effect on the mineral dust longwave, direct radiative forcing, Geophys. Res. Lett., 41(19), 6978–6985, doi:10.1002/2014GL060946, 2014b.

Sicard, M., Barragan, R., Dulac, F., Alados-Arboledas, L. and Mallet, M.: Aerosol optical, microphysical and radiative properties at regional background insular sites in the western Mediterranean, Atmos. Chem. Phys., 16(18), 12177–12203, doi:10.5194/acp-16-12177-2016, 2016.

Stamnes, K., Tsay, S.-C., Wiscombe, W. and Jayaweera, K.: Numerically stable algorithm for discrete-ordinate-method radiative transfer in multiple scattering and emitting layered media, Appl. Opt., 27(12), 2502, doi:10.1364/AO.27.002502, 1988.

Titos, G., del Águila, A., Cazorla, A., Lyamani, H., Casquero-Vera, J. A., Colombi, C., Cuccia, E., Gianelle, V., Močnik, G., Alastuey, A., Olmo, F. J. and Alados-Arboledas, L.: Spatial and temporal variability of carbonaceous aerosols: Assessing the impact of biomass burning in the urban environment, Sci. Total Environ., 578, 613–625, doi:10.1016/j.scitotenv.2016.11.007, 2016.

Torres, B., Dubovik, O., Fuertes, D., Schuster, G., Cachorro, V. E., Lapyonok, T., Goloub, P., Blarel, L., Barreto, A., Mallet, M., Toledano, C., and Tanré, D.: Advanced characterisation of aerosol size properties from measurements of spectral optical depth using the GRASP algorithm, Atmos. Meas. Tech., 10, 3743-3781, https://doi.org/10.5194/amt-10-3743-2017, 2017.

Valenzuela, A., Olmo, F. J., Lyamani, H., Antón, M., Quirantes, A. and Alados-Arboledas, L.: Aerosol radiative forcing during African desert dust events (2005-2010) over Southeastern Spain, Atmos. Chem. Phys., 12(21), 10331–10351, doi:10.5194/acp-12-10331-2012, 2012.

Vogelmann, A. M., Flatau, P. J., Szczodrak, M., Markowicz, K. M. and Minnett, P. J.: Observations of large aerosol infrared forcing at the surface, Geophys. Res. Lett., 30(12), doi:10.1029/2002GL016829, 2003.

Wan, Z.: New refinements and validation of the collection-6 MODIS land-surface temperature/emissivity product, Remote Sens. Environ., 140, 36–45, doi:10.1016/j.rse.2013.08.027, 2014.

Yang, P., Feng, Q., Hong, G., Kattawar, G. W., Wiscombe, W. J., Mishchenko, M. I., Dubovik, O., Laszlo, I. and Sokolik, I. N.: Modeling of the scattering and radiative properties of nonspherical dust-like aerosols, J. Aerosol Sci., 38(10), 995–1014, doi:10.1016/j.jaerosci.2007.07.001, 2007.

Zender, C. S.: Mineral Dust Entrainment and Deposition (DEAD) model: Description and 1990s dust climatology, J. Geophys. Res., 108(D14), 4416, doi:10.1029/2002JD002775, 2003.

Zender, C. S., Miller, R. L. R. L. and Tegen, I.: Quantifying mineral dust mass budgets:Terminology, constraints, and current estimates, Eos, Trans. Am. Geophys. Union, 85(48), 509, doi:10.1029/2004EO480002, 2004.

Tables and figures:

	SW	LW
Spectral range [µm]	0.297 – 3.100	4.5 - 40
Vertical range [km]	0-20	0-100
Number of levels	18	40
Vertical resolution (Vertical range) [km]	0.005 (0-0.01) 0.01 (0.01,0.05) 0.05 (0.05-0.1) 0.1 (0.1-0.2) 0.2 (0.2-1) 1 (1-2) 2 (2-10) 5 (10-20)	 1 (0-25) 2.5 (25-50) 5 (50-60 20 (80-100)

Table 1. Summary of GAME main properties for the SW and LW spectral ranges. The altitude range corresponding to the different vertical resolution values is indicated between parentheses.

		SW			LW		
Surface	**alb**	AERONET			CERES		
	LST	IISTA-CEAMA			MODIS		
Met. prof.	**P,T,RH**	Aircraft + US std atm.			Aircraft + US std atm.		
Main gases	**Conc.**	US std atm.			US std atm.		
	Abs.	HITRAN			HITRAN		
		DS 1	**DS 2**	**DS 3**	**DS 1**	**DS 2**	**DS 3**
Aerosol parameters	**α_{aer}**	GRASP (z, 7 λ)	Klett (z, 3 λ)	Aircraft (z, 1 λ)	Mie calculation		
	SSA	GRASP (z, 7 λ)	AERONET (col, 4 λ)	Aircraft (col, 1 λ)			

	g	AERONET (col, 4 λ)	AERONET (col, 4 λ)	AERONET (col, 4 λ)	

Table 2. Summary of the data sources used to obtain the input data parameterizations for GAME computations both in the SW and LW spectral ranges, including the surface parameters (albedo, *alb*, and Land-surface temperature, LST), profiles of meteorological variables and main gases and the aerosol parameters. For the aerosol parameters (aerosol extinction, α_{aer}, single scattering albedo, SSA, and asymmetry parameter, g) three different datasets are used (DS1, DS2 and DS3) based on different instrumentation and retrievals. The indications below the sources of the aerosol parameters indicate whether the parameter is column integrated (col) or if it is vertically resolved (z) and the number of wavelengths at which it is given (n λ).

	***alb*(440nm)**	***alb*(675nm)**	***alb*(870nm)**	***alb*(1020nm)**	***alb*(LW)**	**LST (K)**
June 16	0.05	0.15	0.30	0.30	0.016	314.5
June 17	0.05	0.15	0.31	0.31	0.013	298.1

Table 3. Surface albedo, *alb(λ)*, values provided by AERONET for the SW spectral range and by CERES for the LW. Land-surface temperature (LST) on June 16 was obtained from MODIS whereas on June 17 was estimated from the meteorological station at Granada site. These surface parameters are common to all parameterizations.

16 June (SZA=31.49º)

	N_f ($\#\cdot\mu m^{-2}$)	N_c ($\#\cdot\mu m^{-2}$)	r_f (µm)	r_c (µm)	σ_f (µm)	σ_c (µm)	AOD (550 nm)
DS1	9.04	0.018	0.12	2.22	0.48	0.73	0.18
DS2	7.53	0.014	0.12	1.90	0.57	0.65	0.23
DS3	-	-	0.11	1.92	0.63	0.66	0.23

17 June (SZA=61.93º)

	N_f ($\#\cdot\mu m^{-2}$)	N_c ($\#\cdot\mu m^{-2}$)	$r_{eff,f}$ (µm)	$r_{eff,c}$ (µm)	σ_f (µm)	σ_c (µm)	AOD (550 nm)
DS1	9.04	0.014	0.10	2.40	0.45	0.72	0.16
DS2	8.03	0.012	0.11	2.08	0.53	0.68	0.19
DS3	-	-	0.11	2.56	0.64	0.59	0.18

Table 4. Column-integrated number concentration (*N*), effective radii (r_{eff}) and standard deviation (σ) of fine and coarse aerosol modes and AOD at 550 nm for DS1, DS2 and DS3 on 16 and 17 June.

Con formato: Subíndice

		LW		
		DS1	**DS2**	**DS3**
Mie calculations	**RI**	DB (2017), (col, 601 λ)	DB (2017), (col, 601 λ)	DB (2017), (col, 601 λ)
	r_{eff}	GRASP (col),	AERONET (col)	Aircraft (z)
	σ	GRASP (col)	AERONET (col)	Aircraft (z)
	N	GRASP (z)	AERONET (col)	Aircraft (z)

Table 5. Summary of the data used to obtain $\alpha_{aer}(\lambda,z)$, SSA(λ,z) and g(λ,z) in the LW from Mie calculations, i.e. the refractive index, RI, effective radius, r_{eff}, geometric standard deviation, σ, and number concentration, *N*. Three different datasets are used (DS1, DS2 and DS3) based on different particle size distribution (PSD) data used. The indications below the sources of the aerosol parameters indicate whether the parameter is column integrated (col) or if it is vertically resolved (*z*) and the number of wavelengths at which it is given (*n λ*). DB(2017) stands for Di Biagio et al., (2017).

	June 16	**June 17**

	$^{BOA}ARE_{SW}$ (W·m^{-2})	$^{TOA}ARE_{SW}$ (W·m^{-2})	$^{BOA}ARE_{SW}$ (W·m^{-2})	$^{TOA}ARE_{SW}$ (W·m^{-2})
DS1	-18.1	-6.3	-27.1	-10.3
DS2	-28.6	-5.5	-34.0	-9.6
DS3	-34.3	-1.5	-35.8	-6.5
Avg ± std. dev	-27.0± 8.2	-4.4±2.6	-32.3±4.6	-8.8±2.0
	June 16		**June 17**	
	^{BOA}FE (W·m^{-2})	^{TOA}FE (W·m^{-2})	^{BOA}FE (W·m^{-2})	^{TOA}FE (W·m^{-2})
DS1	-100.6	-35.0	-169.4	-64.4
DS2	-124.35	-23.9	-178.9	-50.5
DS3	-149.13	-6.52	-198.9	-36.1
Avg ± std. dev				

Tabla con formato

Table 6. ARE at the BOA and the TOA for the SW spectral range obtained with GAME using as inputs DS1, DS2 and DS3 for June 16 and 17, 2013. The averaged values and standard deviation are also included.

	June 16		**June 17**		**ΔAOD**	**Δr_c (μm)**	**$\Delta^{BOA}ARE_{LW}$ (W·m^{-2})**
	$^{BOA}ARE_{LW}$ (W·m^{-2})	$^{TOA}ARE_{LW}$ (W·m^{-2})	$^{BOA}ARE_{LW}$ (W·m^{-2})	$^{TOA}ARE_{LW}$ (W·m^{-2})			
DS1	+3.1	+2.2	+2.6	+1.6	-0.02	+0.18	-0.5
DS2	+3.9	+2.9	+2.9	+1.7	-0.04	+0.18	-1.0
DS3	+2.5	+1.3	+4.1	+1.8	-0.05	+0.64	+1.6
Avg ± std. dev	3.2±0.7	2.1±0.8	3.2±0.8	1.7±0.1			
	June 16		**June 17**				
	^{BOA}FE (W·m^{-2})	^{TOA}FE (W·m^{-2})	^{BOA}FE (W·m^{-2})	^{TOA}FE (W·m^{-2})			
DS1	±17.2	±12.2	±16.3	±10.0			
DS2	±17.0	±12.6	±15.3	±8.9			
DS3	±10.9	±5.7	±22.8	±10.0			
Avg ± std. dev							

Comentado [MJ3]: Comentar FE en el texto y mejorar tabla

Table 7. ARE at the BOA and the TOA for the LW spectral range obtained with GAME using as inputs DS1, DS2 and DS3 for June 16 and 17, 2013. The averaged values and standard deviation are also included. The last three columns include variations (Δ) of AOD, r_c and ARE at the BOA between June 16 an 17 for the three datasets.

	June 16		June 17	
	^{BOA}ARE (W·m^{-2})	^{TOA}ARE (W·m^{-2})	^{BOA}ARE (W·m^{-2})	^{TOA}ARE (W·m^{-2})
DS1	-15.0	-4.5	-24.6	-8.6
DS2	-24.7	-3.1	-31.1	-7.8
DS3	-31.71	-0.1	-31.8	-4.6
Avg ± std. dev	-23.8±8.4	-2.6±2.2	-29.2±4.0	-7.0±2.1
	June 16		**June 17**	
	^{BOA}FE (W·m^{-2})	^{TOA}FE (W·m^{-2})	^{BOA}FE (W·m^{-2})	^{TOA}FE (W·m^{-2})
DS1	-83.3	-25.0	-153.8	-53.8
DS2	-107.4	-13.5	-163.7	-41.1
DS3	-137.9	-0.4	-176.7	-25.6
Avg ± std. dev				

Tabla con formato

Table 8. ARE at the BOA and the TOA for the total (SW+LW) spectral range obtained with GAME using as inputs DS1, DS2 and DS3 for June 16 and 17, 2013. The averaged values and standard deviation are also included.

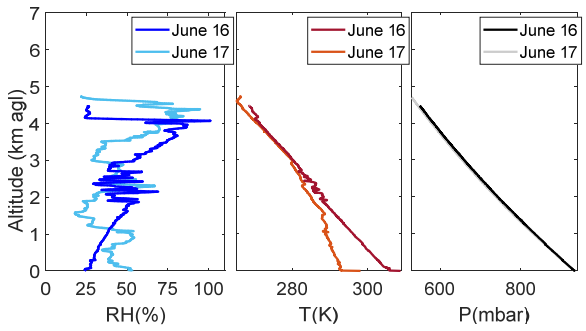

Figure 1. Relative humidity (RH), temperature (T) and pressure (P) profiles measured on-board the ATR during flights F30 (June 16) and F31 (June 17).

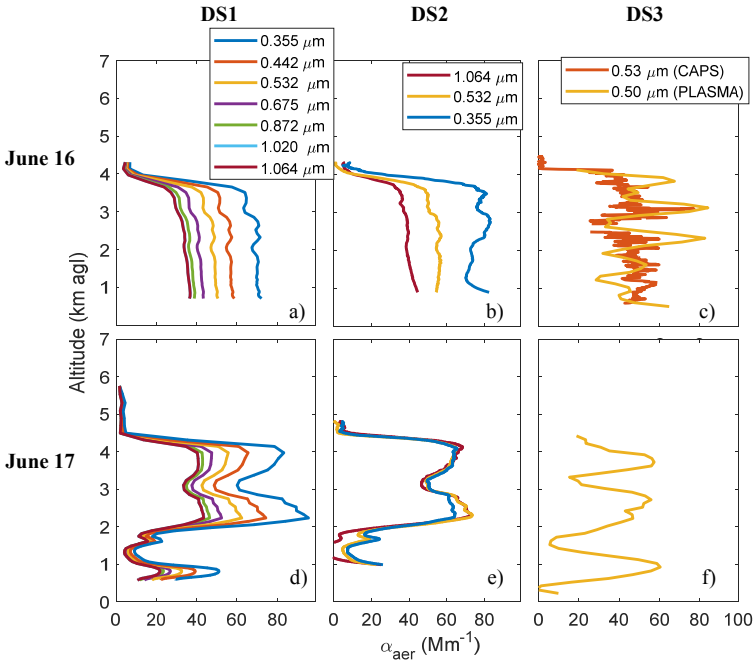

Figure 2. Profiles of α_{aer} obtained from GRASP/DS1 (left), Klett/DS2 (center) and aircraft in-situ/DS3 measurements (right) on June 16 (top row) and June 17 (bottom row).

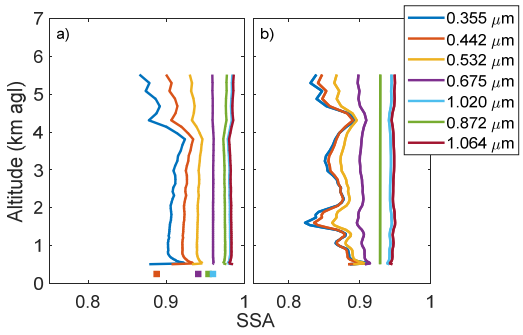

Figure 3. SSA profiles obtained from GRASP/DS1 on June 16 (a) and June 17 (b).

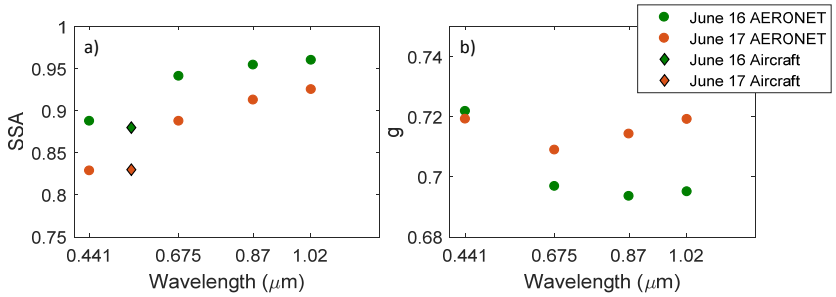

Figure 4. a) AERONET/DS2 column-integrated (circles) and aircraft/DS3 averaged (diamonds) SSA values on June 16 at 16:22UTC and June 17 at 07:20UTC. b) AERONET g values for the same periods.

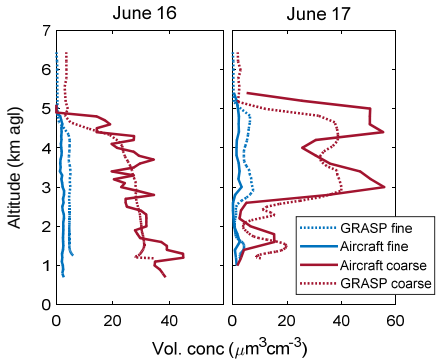

Figure 5. Profiles of aerosol volume concentration for the fine (blue) and coarse (red) mode obtained from GRASP/DS1 (dotted line), and aircraft in-situ/DS3 measurements (solid line) on June 16 (left) and June 17 (right).

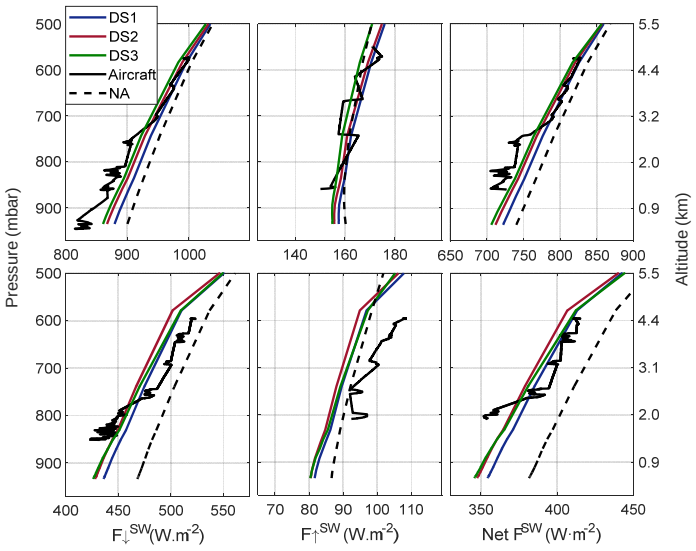

Figure 6. Radiative fluxes for the SW spectral range for June 16 (upper row) and 17 (bottom row) simulated with GAME using different input aerosol datasets (DS1 in blue, DS2 in red and DS3 in green). The black lines are the aircraft in situ measurements distant from about 20 km. The black dashed lines represent the radiative fluxes without the aerosol component (NA).

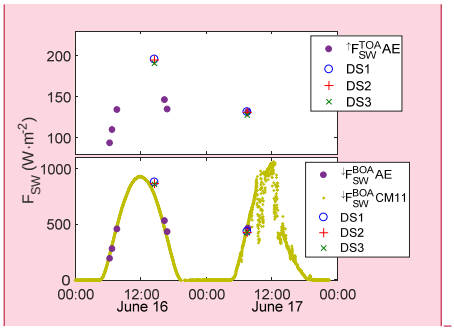

Figure 7. Time series of the $^{\uparrow}F_{SW}$ at the TOA (top) and $^{\downarrow}F_{SW}$ at the BOA (bottom) for the period June 16-17. The green line represents surface measurements from the ground-based pyranometer at Granada station, purple dots are AERONET fluxes, ~~black dots are CERES data~~ and GAME ouput data for different inputs are represented by the blue circles (DS1), red (DS2) and green (DS3) crosses.

Comentado [MJ4]: Quitar CM11? Incluir los datos de las siumulaciones a la hora de las medidas de AERONET

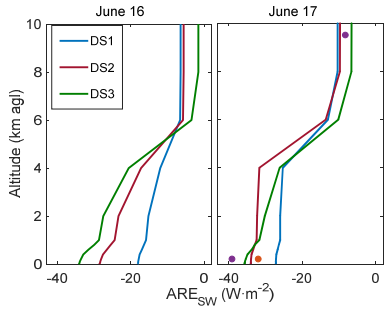

Figure 8. ARE profiles in the SW spectral range simulated using DS1 (blue line), DS2 (red line) and DS3 (green line) as aerosol input data in GAME for June 16 (left) and June 17 (right). The purple dots represent the ARE provided by AERONET (AE) at the BOA and the TOA and the orange dot, the AERONET corrected for the surface albedo effect (AE-C; see text) ARE at the BOA.

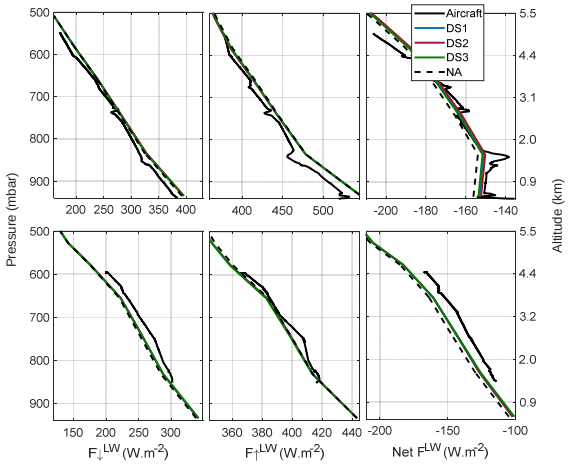

Figure 9. Radiative fluxes for the LW spectral range for June 16 (upper row) and 17 (bottom row) simulated with GAME using different input aerosol datasets (DS1 in blue, DS2 in red and DS3 in green). The black line represents the aircraft in situ measurements. The black dashed lines represent the radiative fluxes without the aerosol component (NA).

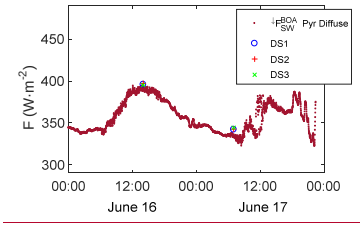

Figure 10. Time series of the ~~global $^{\downarrow}F_{LW}$ at the TOA (top) and the diffuse~~ $^{\downarrow}F_{LW}$ at the BOA ~~(bottom)~~ during the period June 16-17. Surface measurements of diffuse (red) radiation from the ground-based pyranometer at Granada station are included. ~~Black dots are CERES data and~~ GAME ouput data for different inputs are represented by the blue circles (DS1), red (DS2) and green (DS3) crosses.

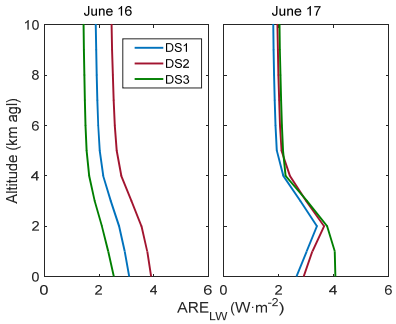

Figure 11. Direct ARE profiles in the LW spectral range simulated using DS1 (blue line), DS2 (red line) and DS3 (green line) as aerosol input data in GAME for June 16 (left) and June 17 (right).

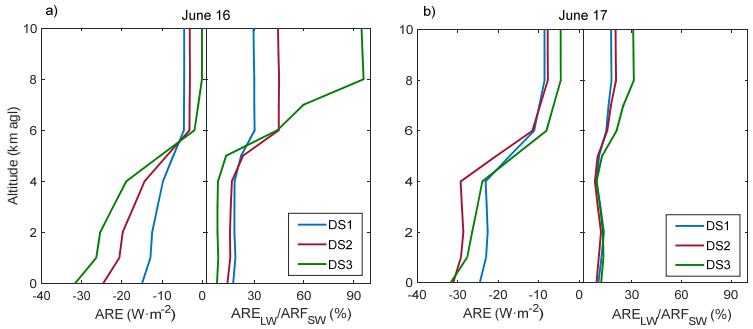

Figure 12. Direct ARE for the total spectrum (left) and the ratio between the ARE LW and the ARE SW in percentage for DS1 (blue), DS2 (red) and DS3 (green) on June 16 at 14:30 UTC (a) and June 17 at 07:30 UTC (b)